Pushing the Limit (Cycle)

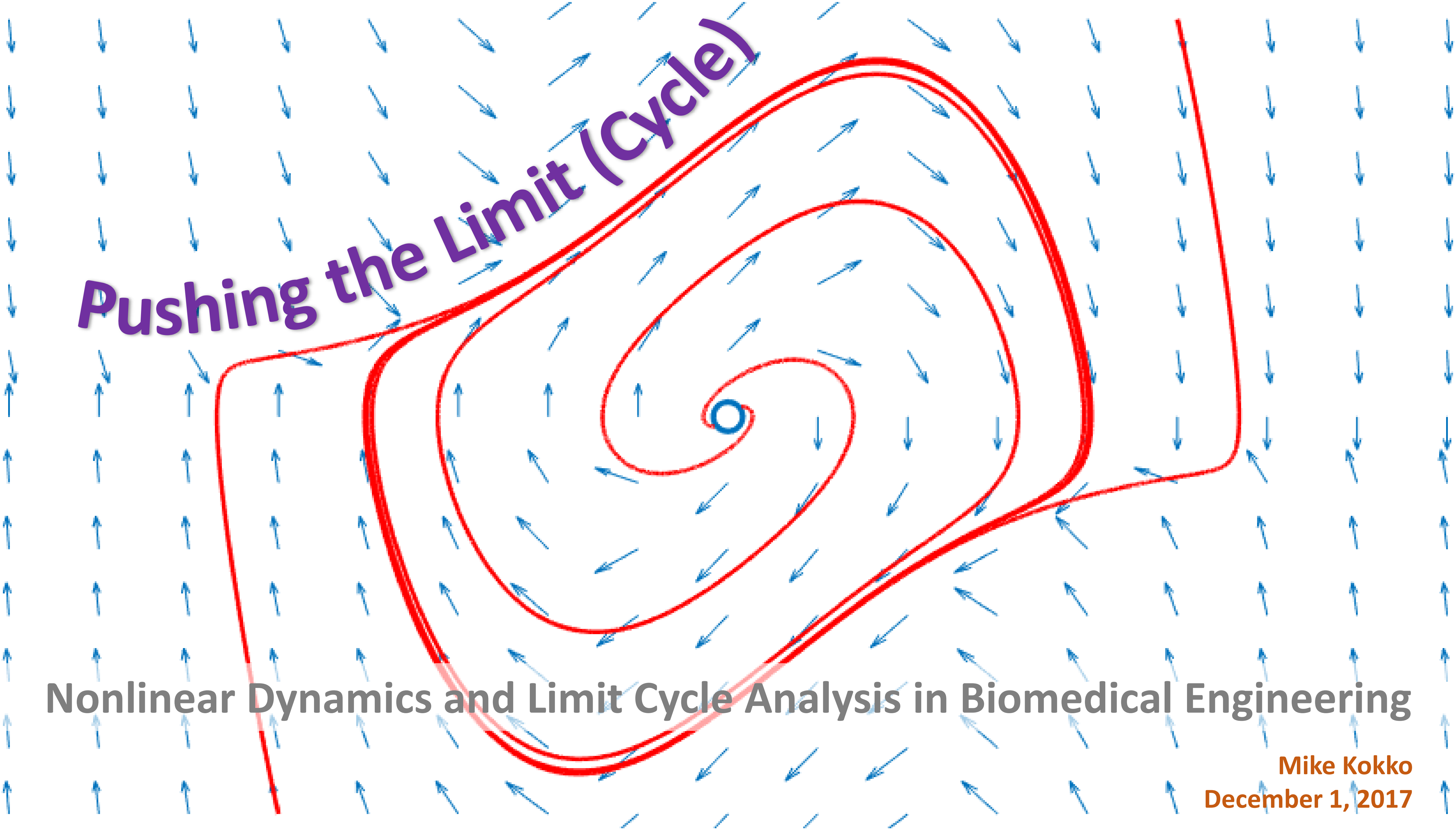

Nonlinear Dynamics and Limit Cycle Analysis in Biomedical Engineering

Mike Kokko

December 1, 2017

Selected Reference Texts

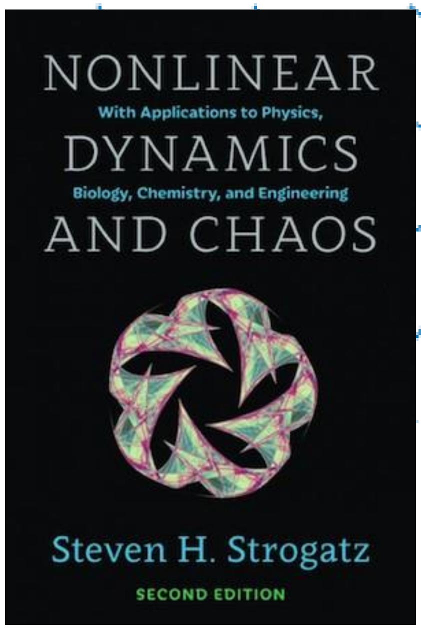

http://www.stevenstrogatz.com

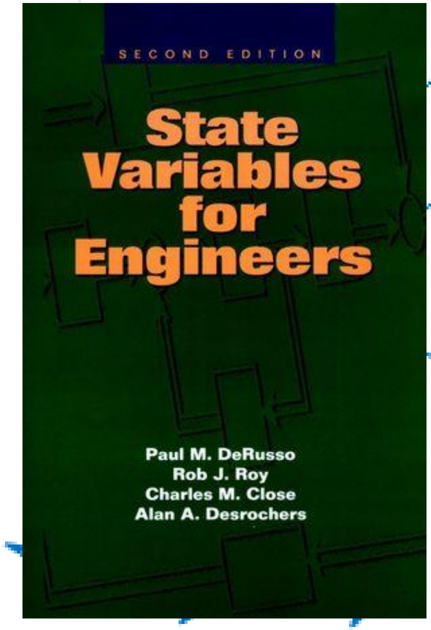

http://www.wiley.com/

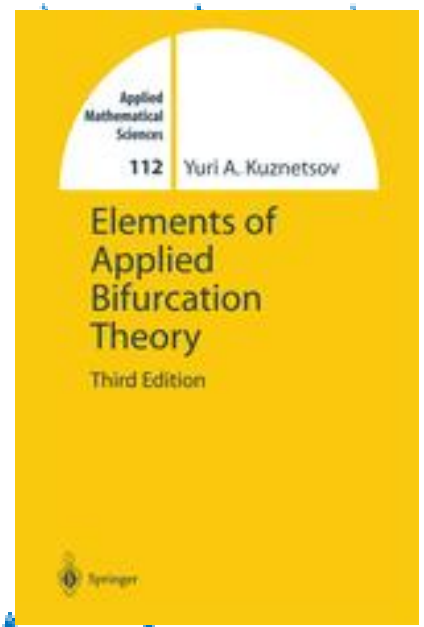

http://www.springer.com/

Strogatz, S.H., *Nonlinear dynamics and chaos : with applications to physics, biology, chemistry, and engineering*. Second edition. ed. 2015, Boulder, CO: Westview Press. xiii, 513 pages.

DeRusso, P.M. and P.M. DeRusso, *State variables for engineers*. 2nd ed. 1998, New York: Wiley. xii,575 p.

Kuznetsov, Y.A., *Elements of applied bifurcation theory*. 2nd ed. Applied mathematical sciences. 1998, New York: Springer. xix, 591 p.

Pushing the Limit (Cycle)

Part I: Theory and Methods

- Linear Dynamics
- Nonlinear Dynamics
  - Phase Portraits
  - Limit Cycle Analysis (Poincare Maps)

Part II: Examples from Biomedical Literature

https://images-na.ssl-images-amazon.com/images/I/41ftha-1oBL.jpg

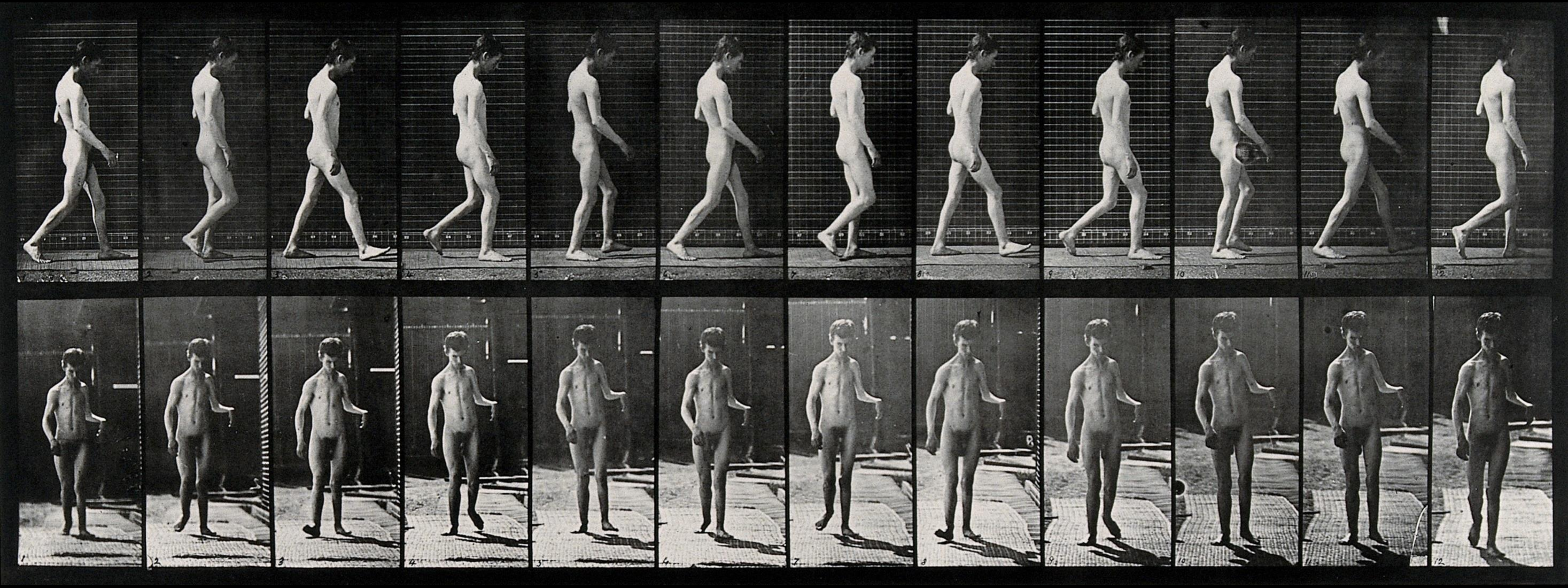

Eadweard Muybridge, 1887. Wikimedia Commons.

http://luxreview.com/upload/system/2016/05/11175406.jpg

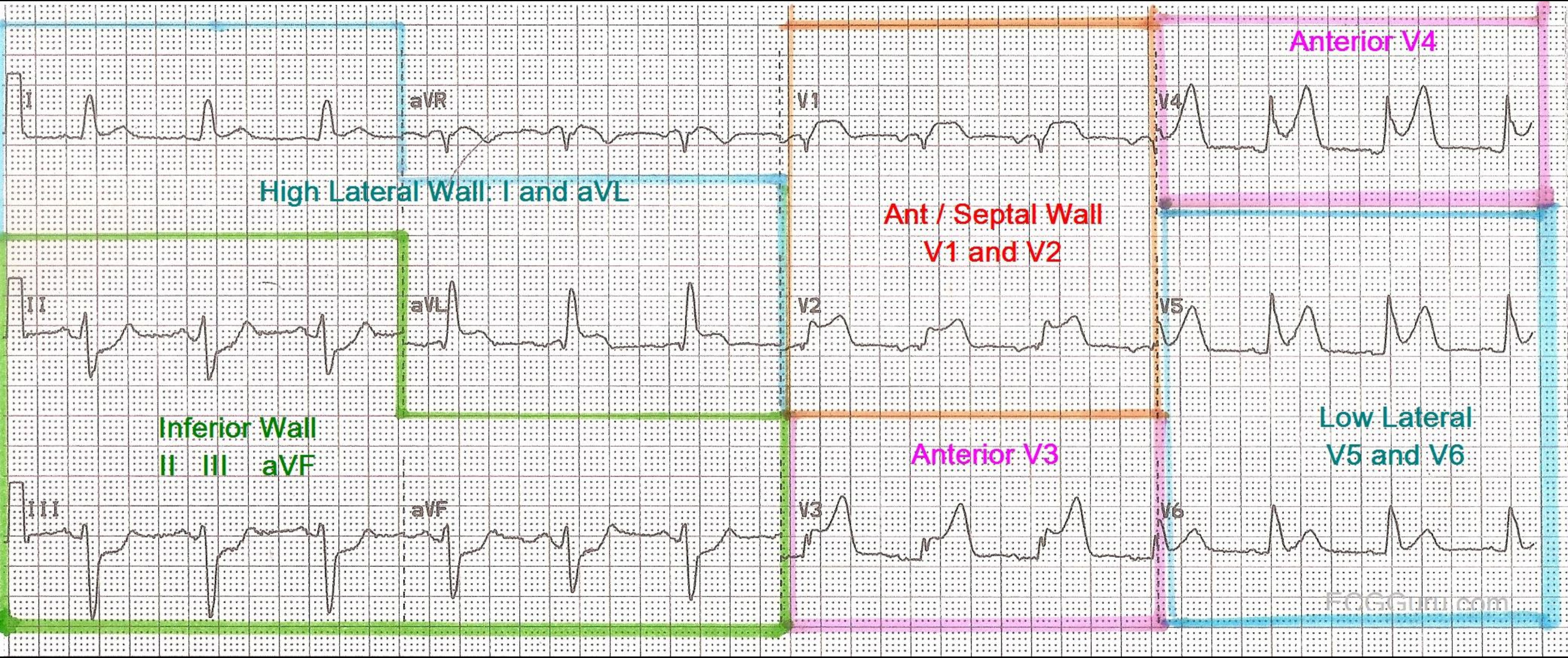

https://www.ecgguru.com/sites/default/files/resource-docs/Mapped%20ECG_0.jpg

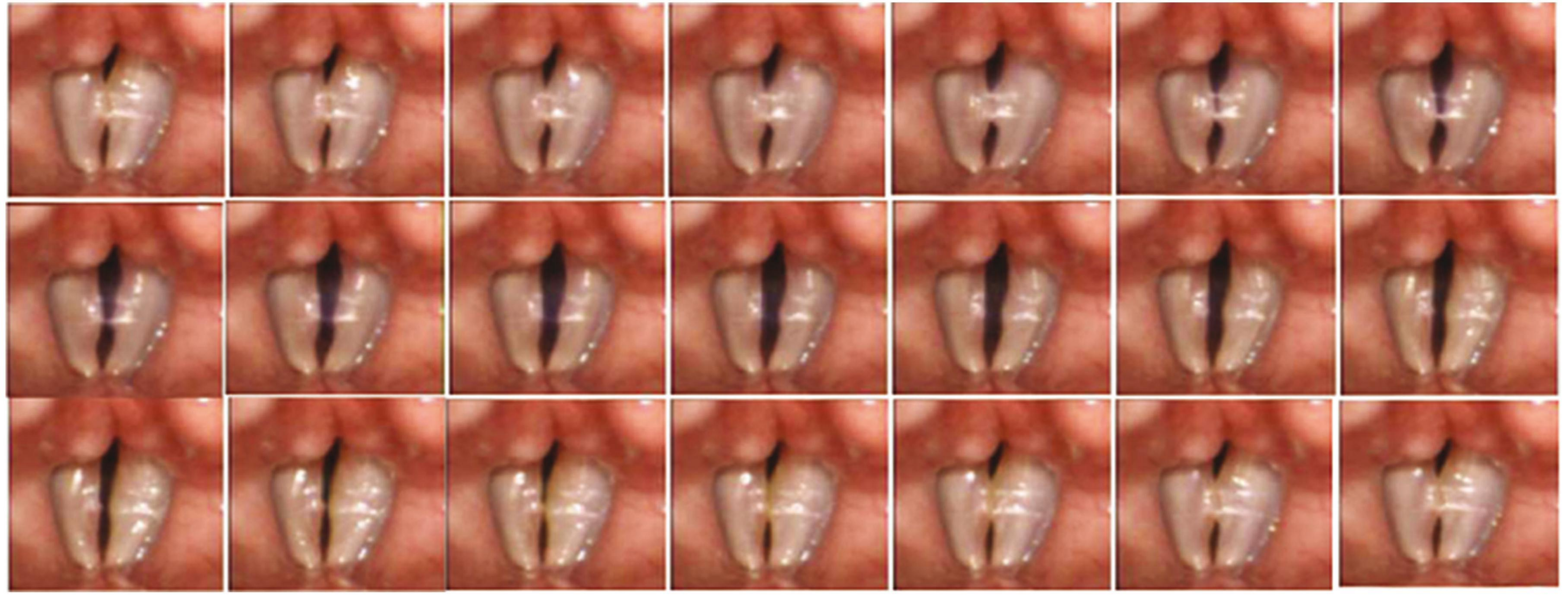

Tsuji, D.H., et al., *Improvement of vocal pathologies diagnosis using high-speed videolaryngoscopy.* Int Arch Otorhinolaryngol, 2014. **18**(3): p. 294-302.

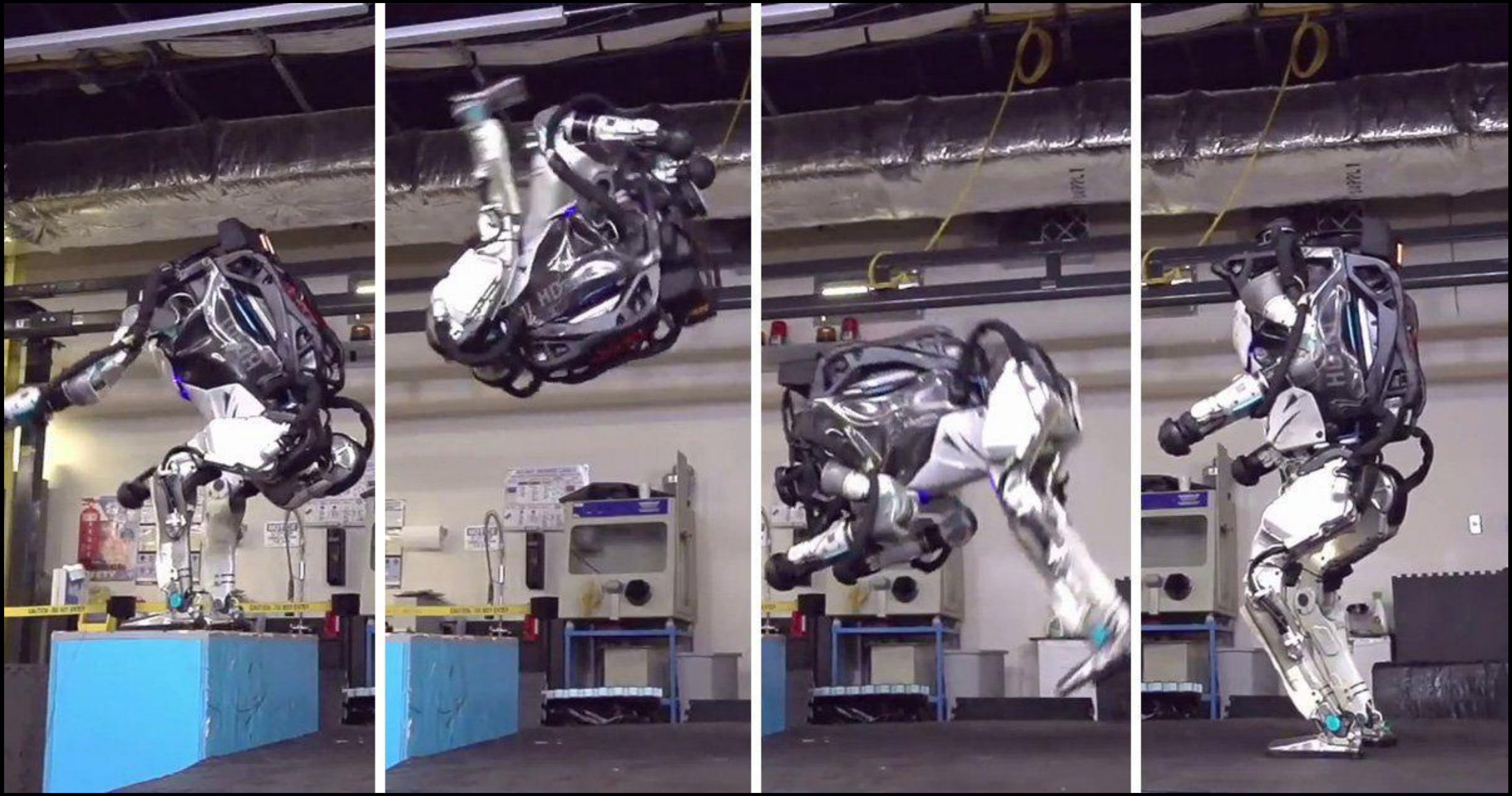

Atlas. Boston Dynamics. https://metrouk2.files.wordpress.com/2017/11/prc_60252175.jpg

Model **Solve**

Physical System → Differential Equation → Full Trajectory

Nonlinear vs. Linearized Pendulum

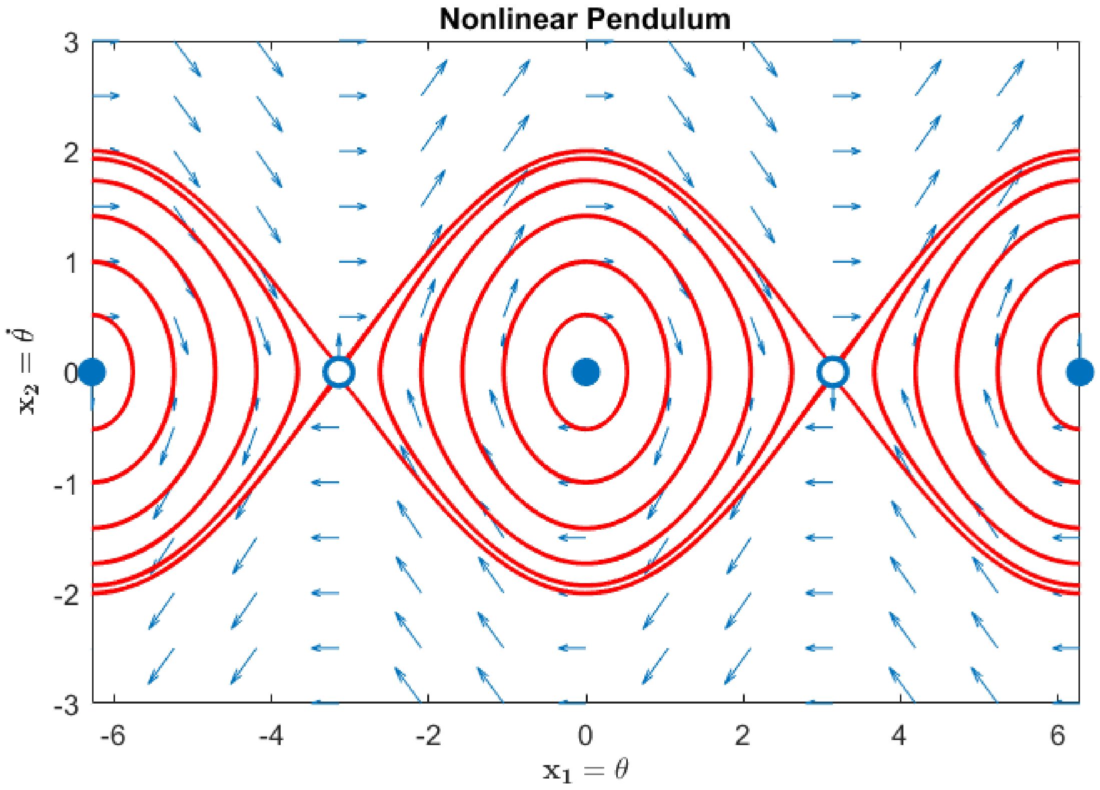

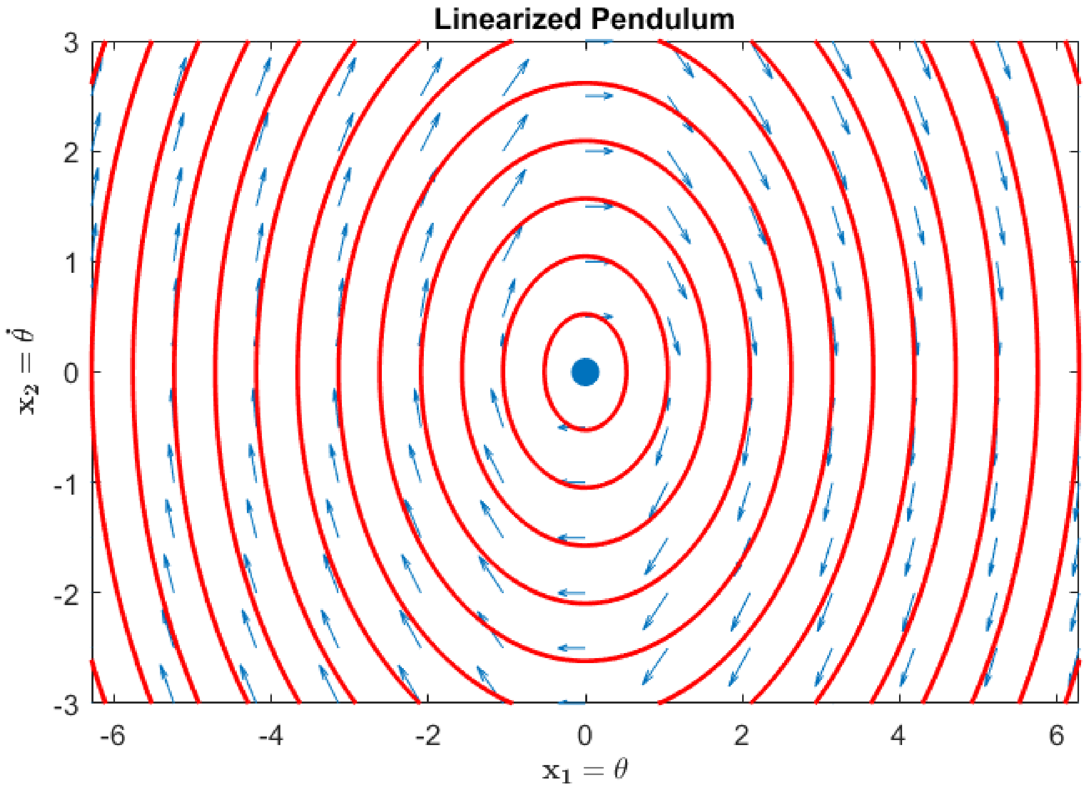

Fixed Point Classification

$$\dot{x} \approx Ax$$

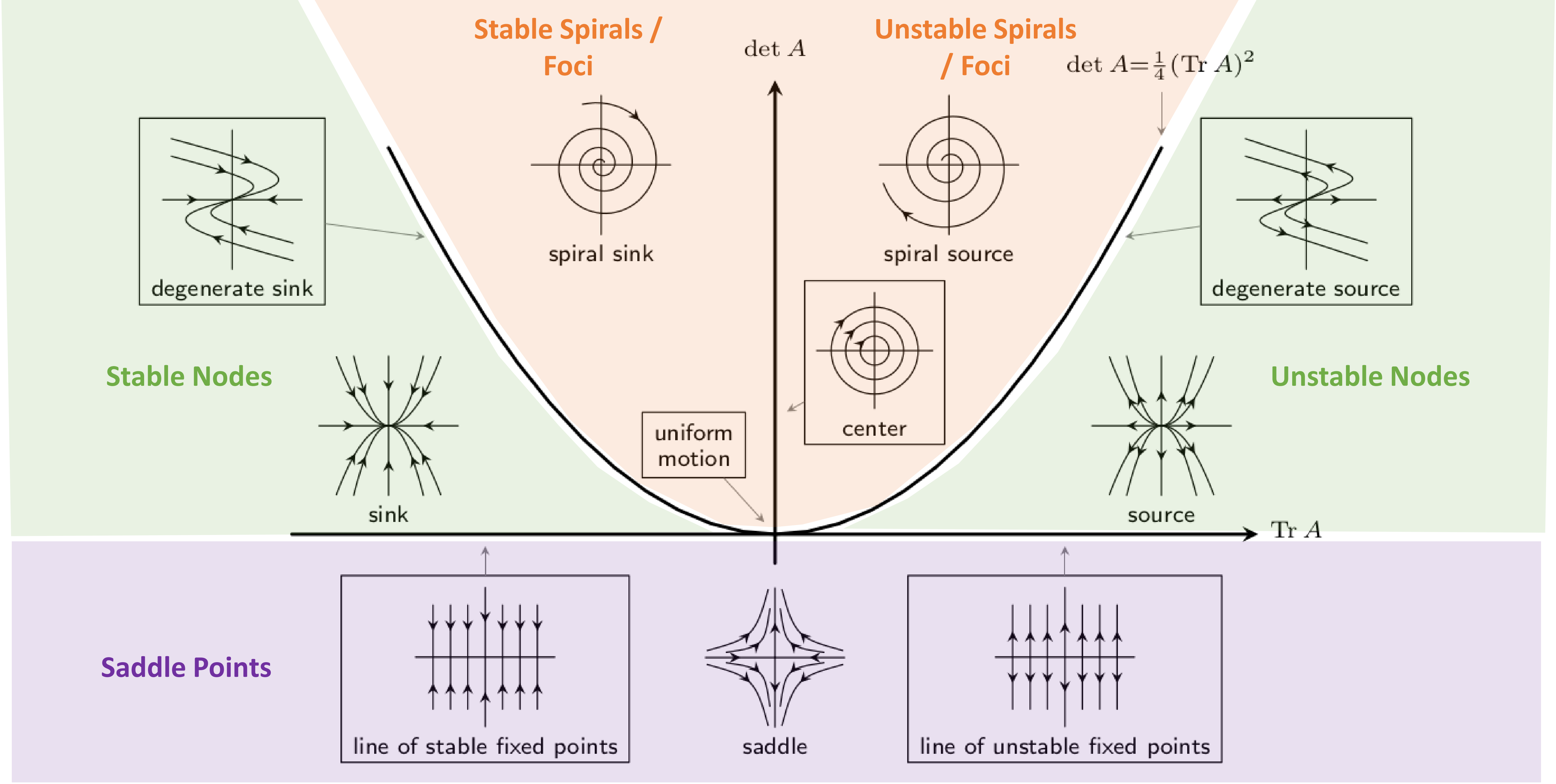

https://i.stack.imgur.com/duPPi.png

Limit Cycles

- **Isolated**, closed orbits in phase plane (state space)
- Only possible in nonlinear systems
- Proving (or ruling out) existence in a region can be tricky
  - Gradient field?
  - Lyapunov function?
  - Dulac's criterion?
  - Poincaré-Bendixson theorem?
- Stable, semi-stable, or unstable

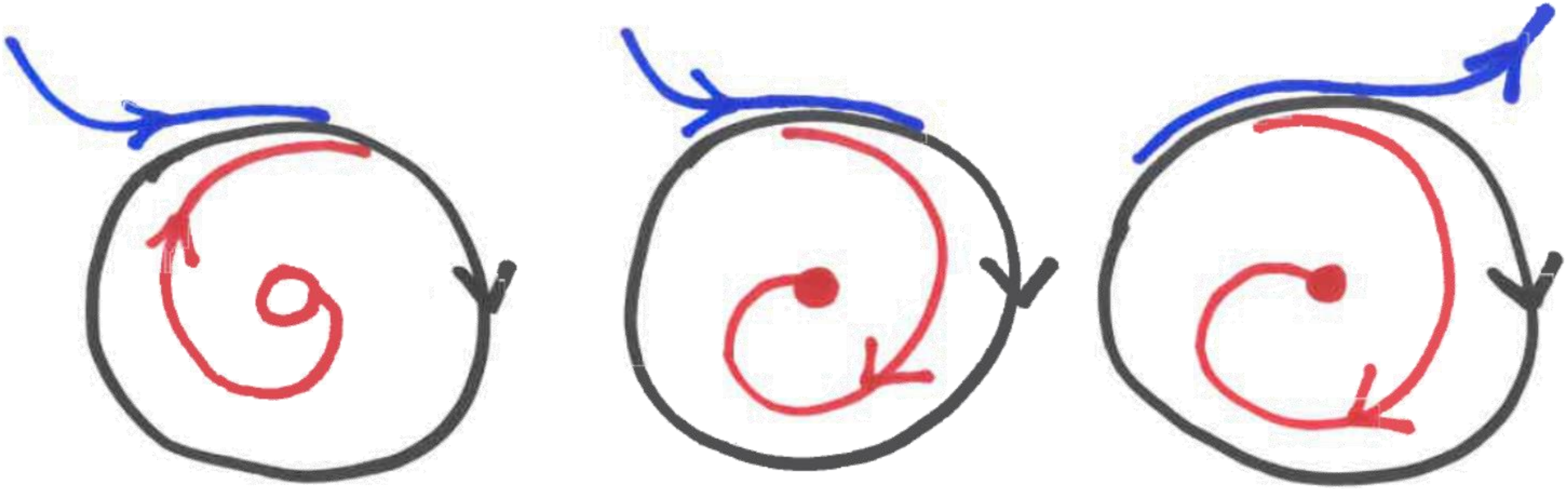

Stable **Semi-Stable** **Unstable**

van der Pol Oscillator Limit Cycle (μ = 1.0)

$$\ddot{x} + \mu\left(x^2 - 1\right)\dot{x} + x = 0$$

$$\dot{\boldsymbol{x}} = \begin{bmatrix}\dot{x}_1\\ \dot{x}_2\end{bmatrix} = \begin{bmatrix} x_2 \\ -\mu\left(x_1^2 - 1\right)x_2 - x_1\end{bmatrix}$$

Balthasar van der Pol
1889 - 1959

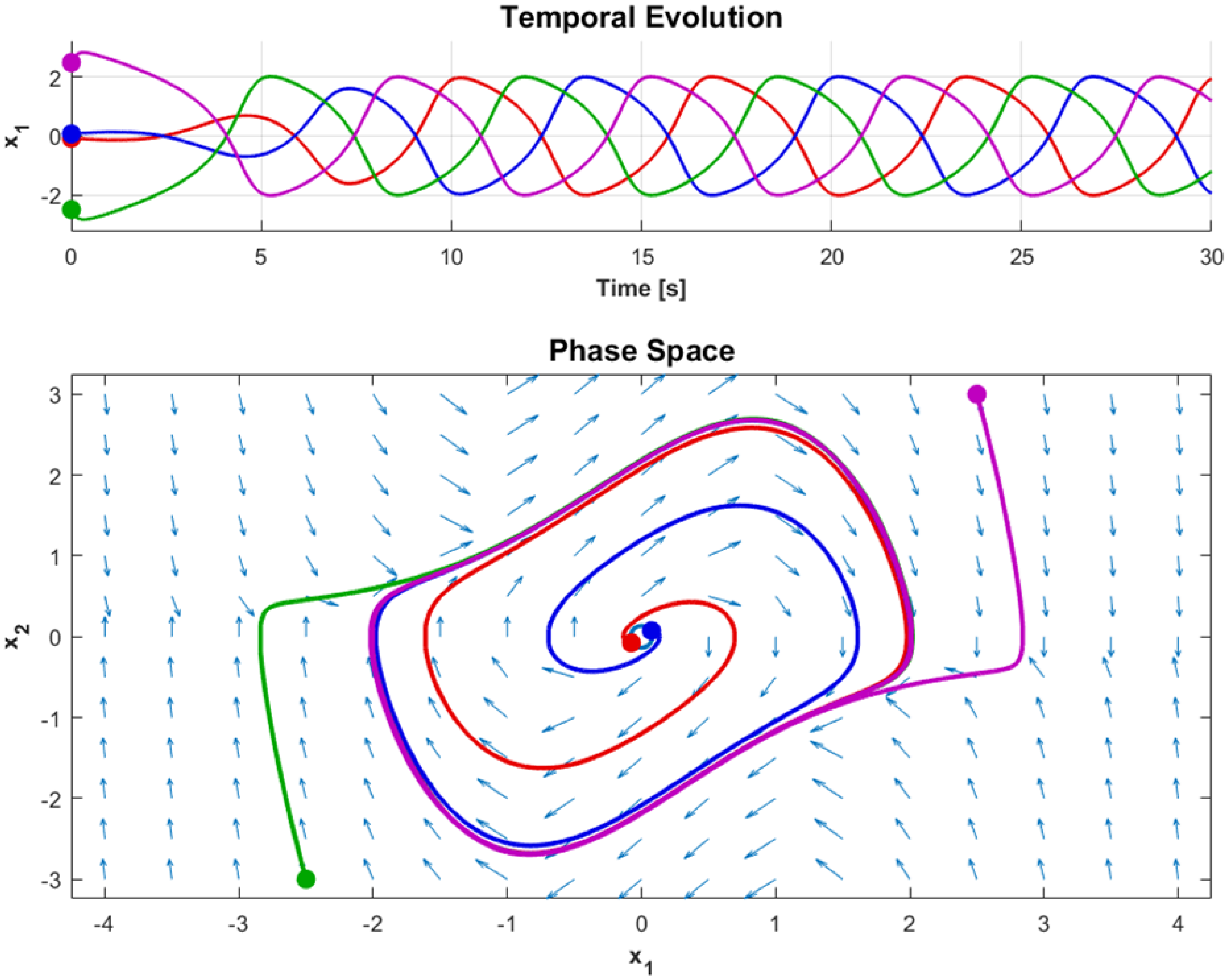

http://www.dos4ever.com/centenial/centenial_en.html

van der Pol Oscillator Limit Cycle (μ = 0.2)

$$\ddot{x} + \mu\left(x^2 - 1\right)\dot{x} + x = 0$$

$$\dot{\boldsymbol{x}} = \begin{bmatrix} \dot{x}_1 \\ \dot{x}_2 \end{bmatrix} = \begin{bmatrix} x_2 \\ -\mu\left(x_1^2 - 1\right)x_2 - x_1 \end{bmatrix}$$

Balthasar van der Pol
1889 - 1959

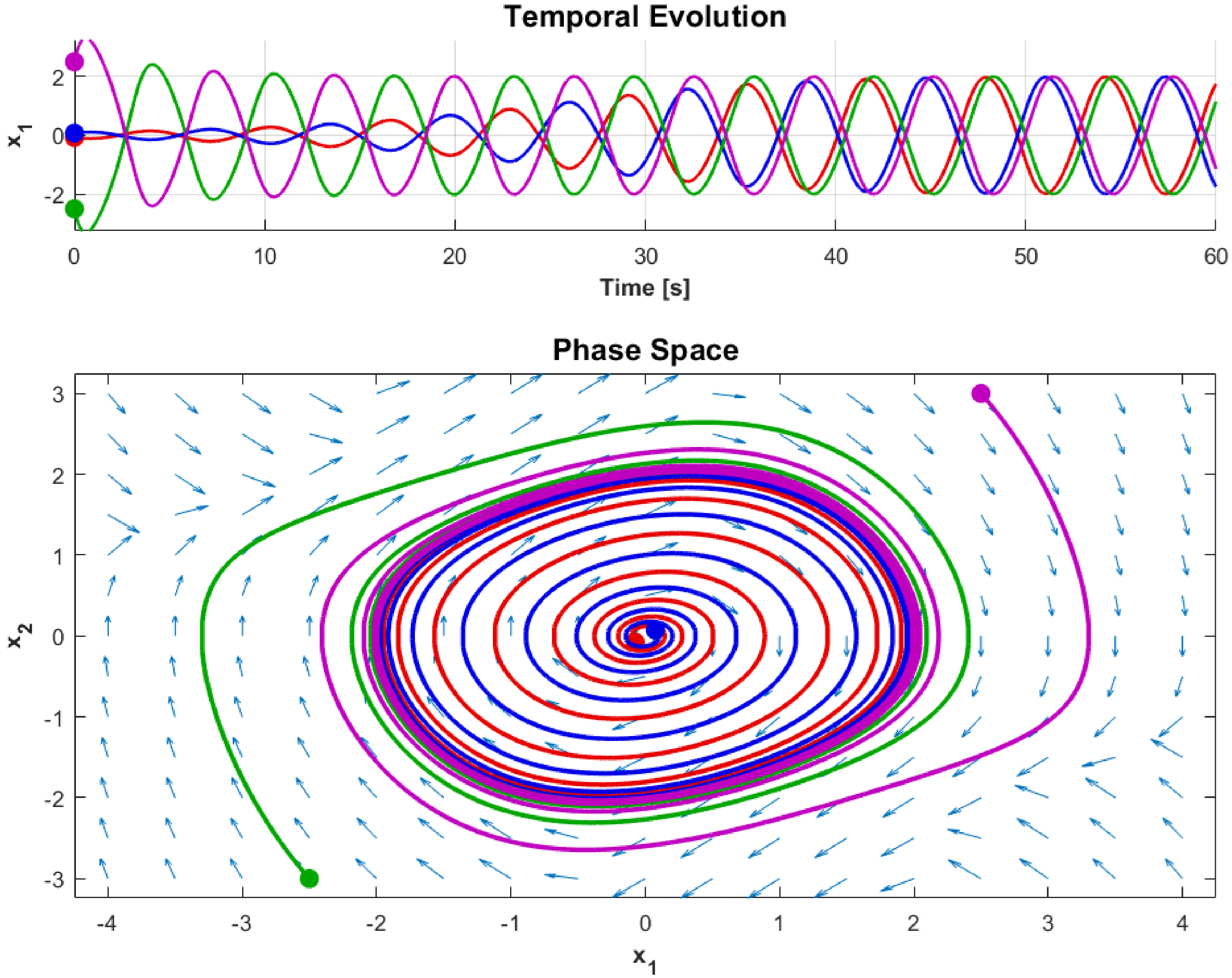

http://www.dos4ever.com/centenial/centenial_en.html

Poincaré Maps

- First return map relative to a **surface of section S** (P: $\mathbb{R}^{n-1} \rightarrow \mathbb{R}^{n-1}$)
- In $\mathbb{R}^2$ fixed points and closed orbits fall on the line of slope 1
- "Easily" extended to higher dimensions
- Continuous time system becomes discrete $\{\dot{\boldsymbol{x}} = f(\boldsymbol{x})\} \rightarrow \{\boldsymbol{x}_{k+1} = P(\boldsymbol{x}_k)\}$
- Stability related to eigenvalues of linearized P (slope < 1 in $\mathbb{R}^2$)

Henri Poincaré
1854 - 1912

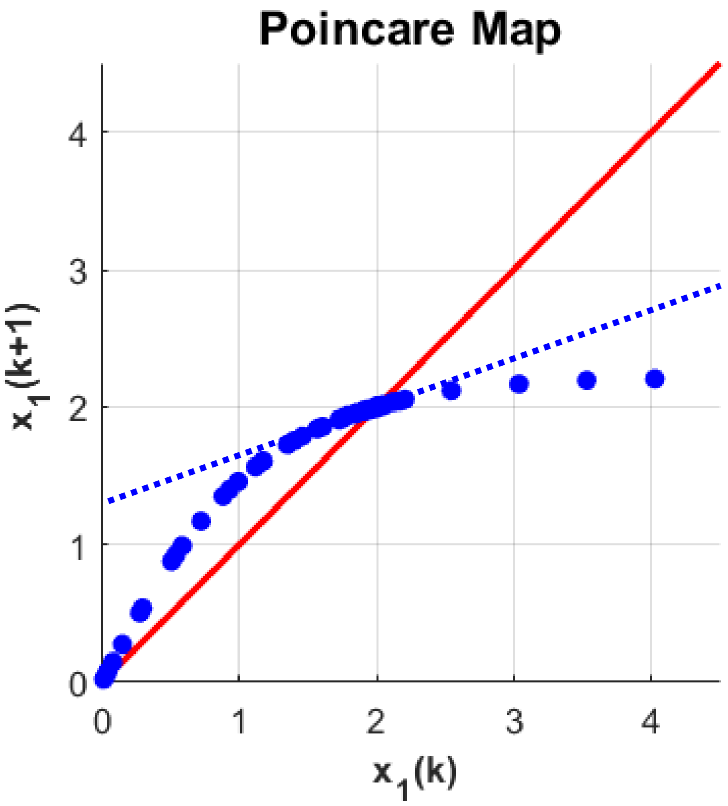

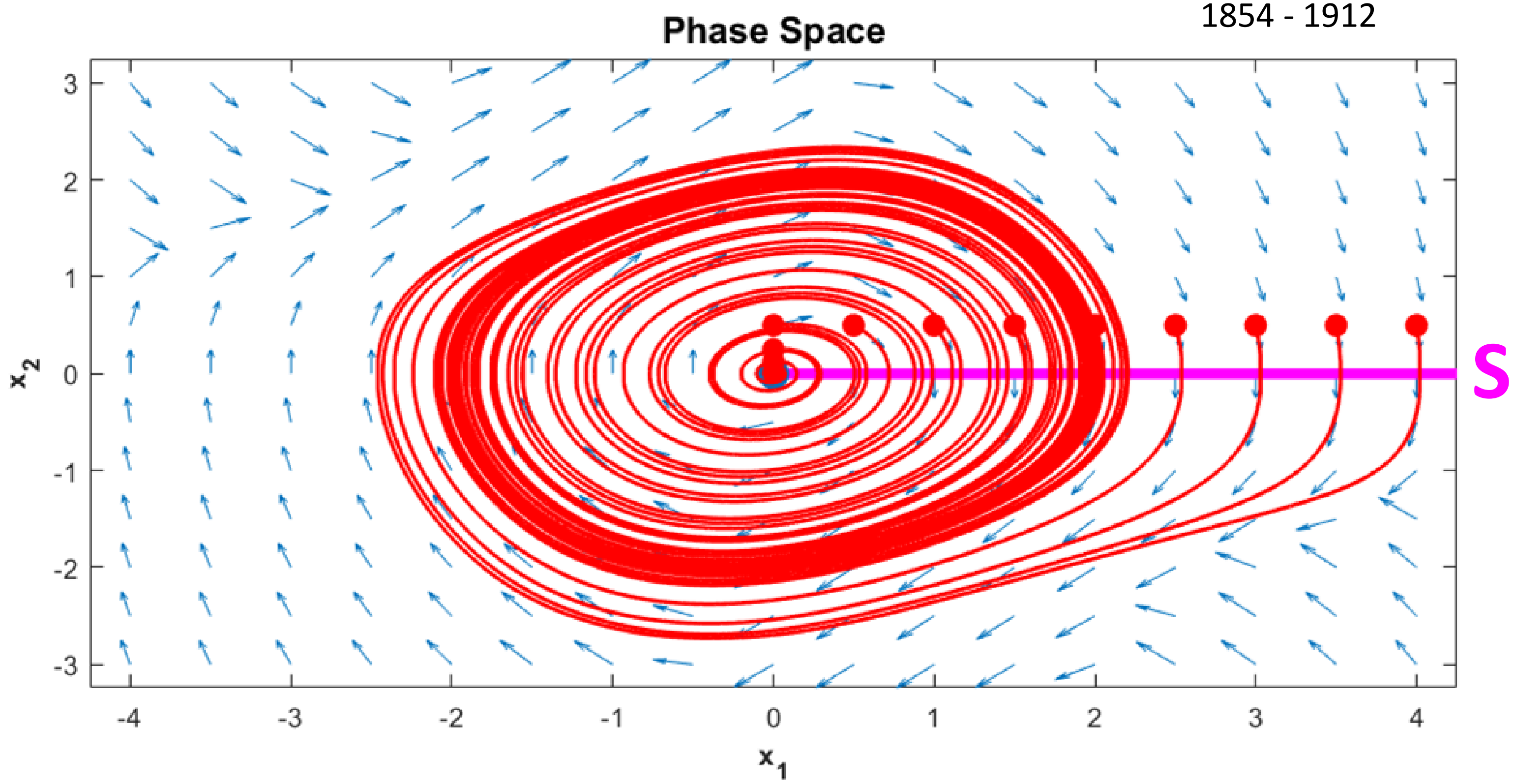

http://underactuated.mit.edu/underactuated.html?chapter=4 http://www.mlahanas.de/Physics/Bios/images/HenriPoincare.jpg

Poincaré Maps

- First return map relative to a **surface of section S** ($P: \mathbb{R}^{n-1} \rightarrow \mathbb{R}^{n-1}$)
- In $\mathbb{R}^2$ fixed points and closed orbits fall on the line of slope 1
- "Easily" extended to higher dimensions
- Continuous time system becomes discrete $\{\dot{\boldsymbol{x}} = f(\boldsymbol{x})\} \rightarrow \{\boldsymbol{x}_{k+1} = P(\boldsymbol{x}_k)\}$
- Stability related to eigenvalues of linearized P (slope < 1 in $\mathbb{R}^2$)

Henri Poincaré
1854 - 1912

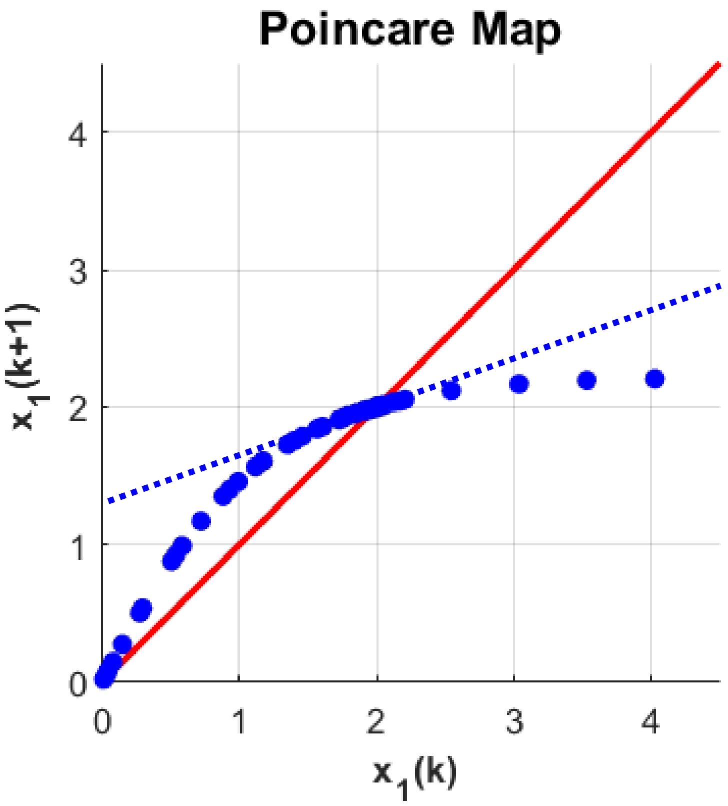

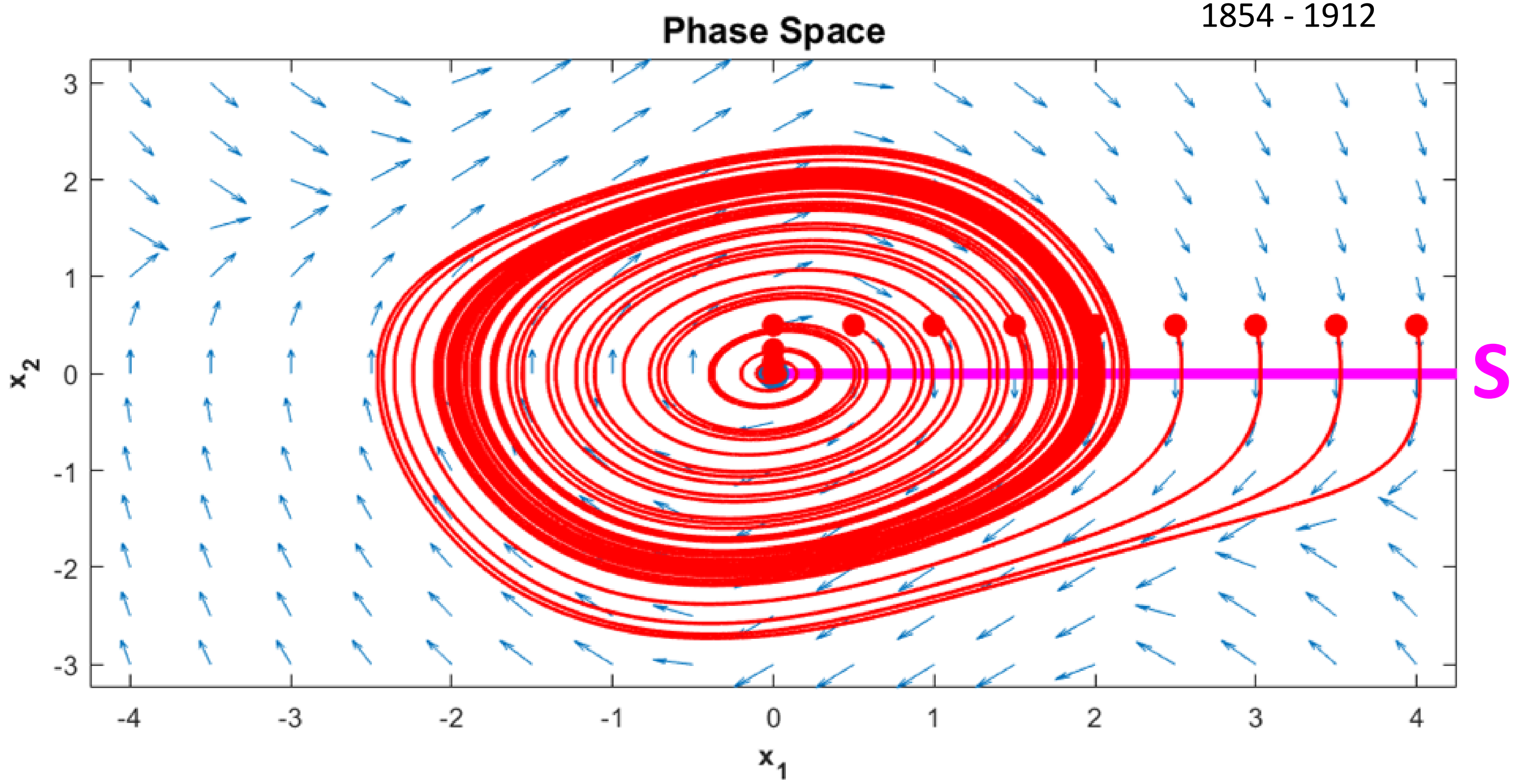

http://underactuated.mit.edu/underactuated.html?chapter=4 http://www.mlahanas.de/Physics/Bios/images/HenriPoincare.jpg

Gait Cycle Analysis

Phase Plane Analysis, Limit Cycles, Poincaré Maps

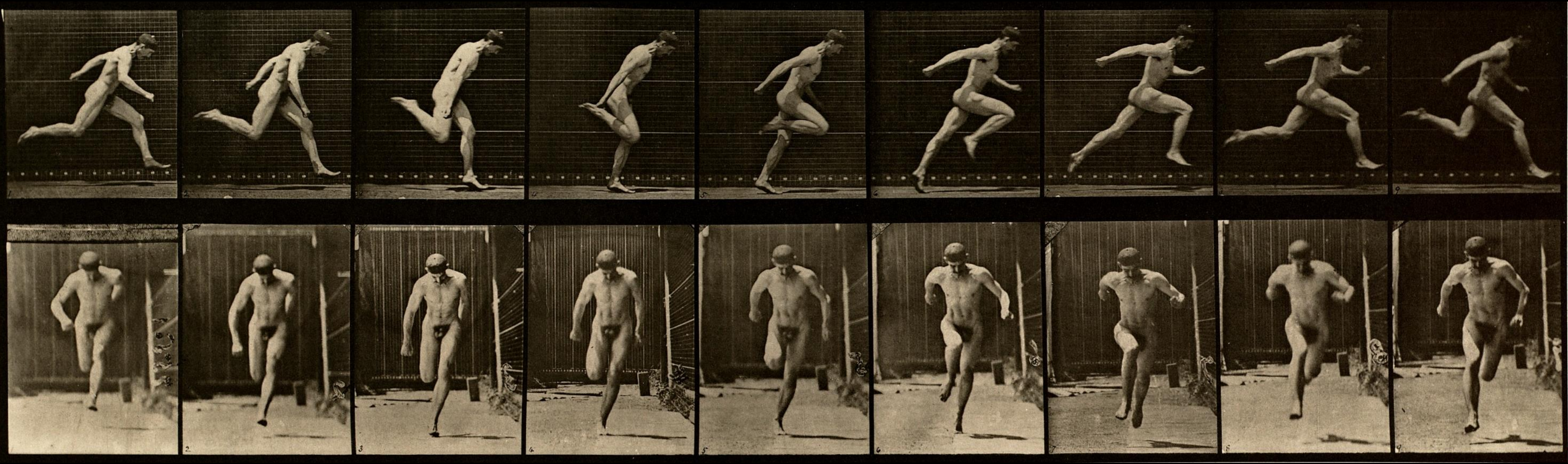

Eadweard Muybridge, 1887. Wikimedia Commons.

Gait Cycle Analysis

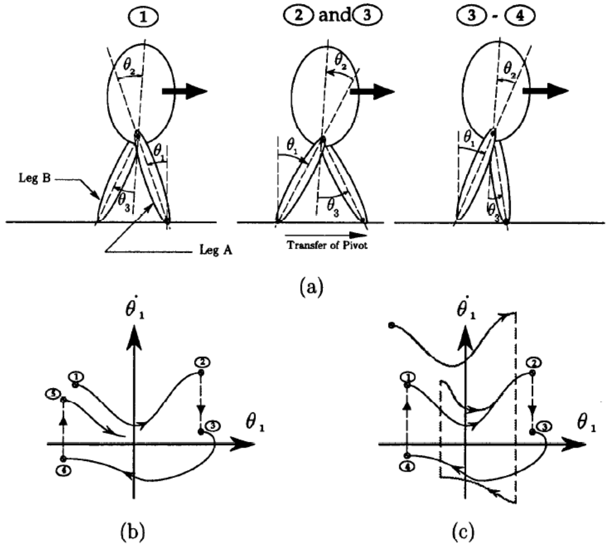

Fig. 1. Phase plane portrait and periodic motions of a three-link model.

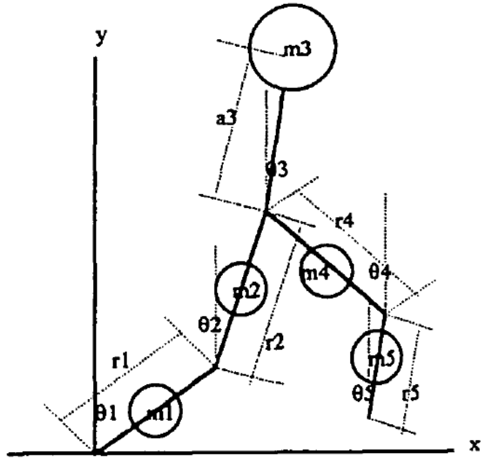

Fig. 1. Five-link biped robot.

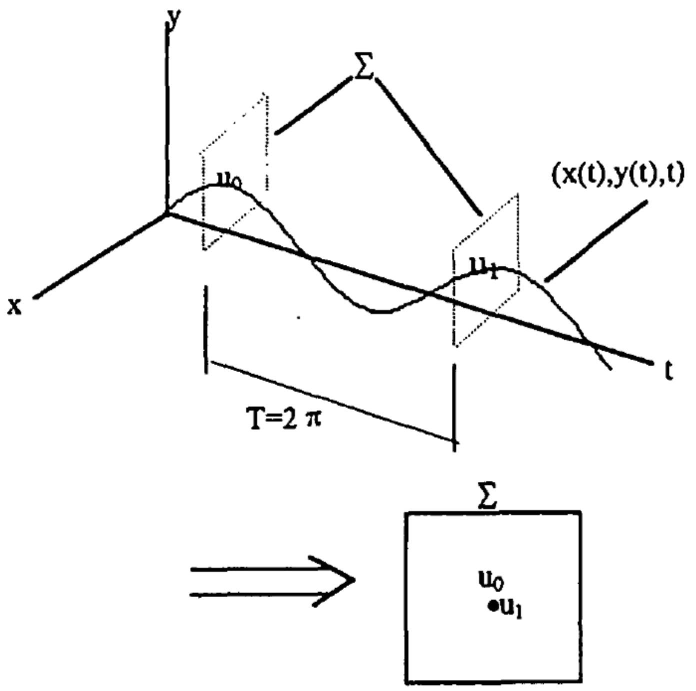

Fig. 2. Poincaré map for a continuous system.

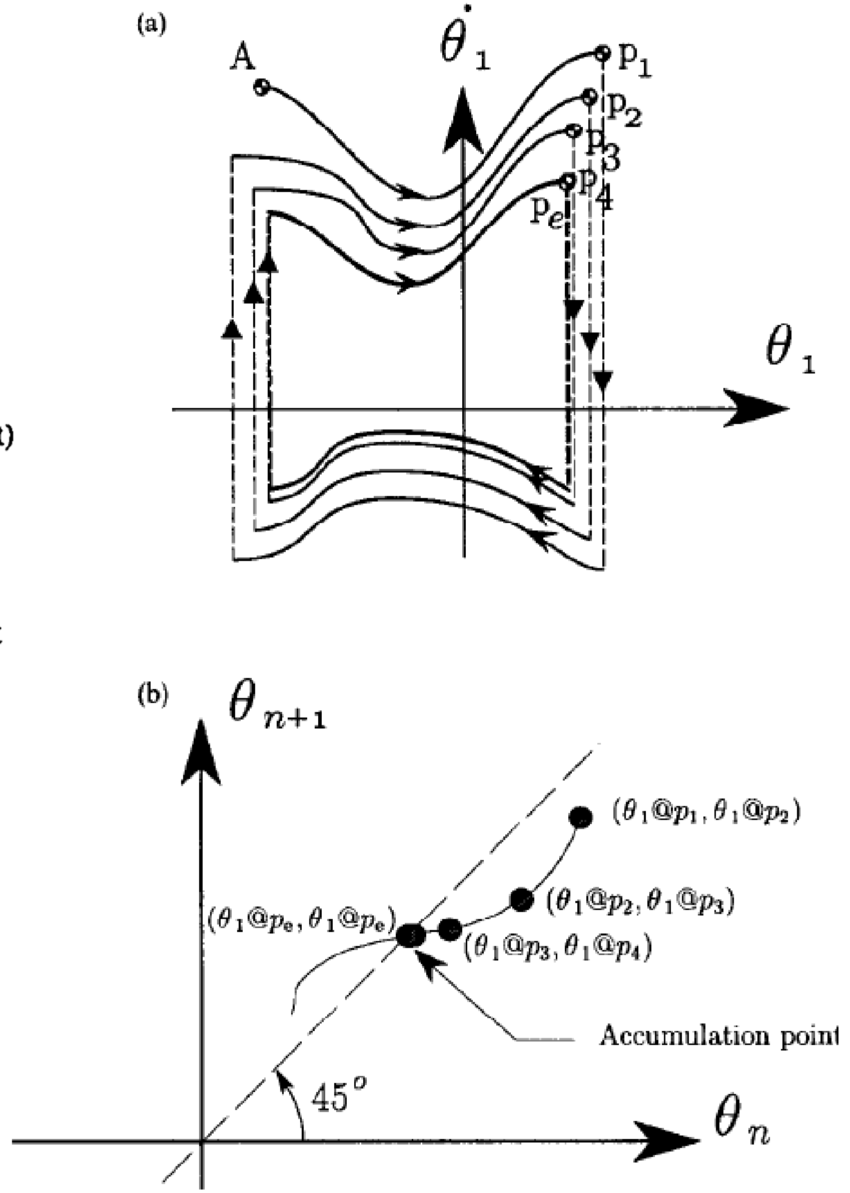

Fig. 2. Equilibrium points and the first return map.

Hurmuzlu, Y., C. Basdogan, and J.J. Carollo, *Presenting joint kinematics of human locomotion using phase plane portraits and Poincare maps.* J Biomech, 1994. **27**(12): p. 1495-9.
Cheng, M.Y. and C.S. Lin, *Measurement of robustness for biped locomotion using a linearized Poincare map.* Robotica, 1996. **14**: p. 253-259.

Gait Cycle Analysis

ϕ_1, ϕ_4, ϕ_7 — sagittal plane excursion of ankle, knee, and hip joints, respectively.

ϕ_2, ϕ_5, ϕ_8 — coronal plane excursion of ankle, knee, and hip joints, respectively.

ϕ_3, ϕ_6, ϕ_9 — transverse plane excursion of ankle, knee, and hip joints, respectively.

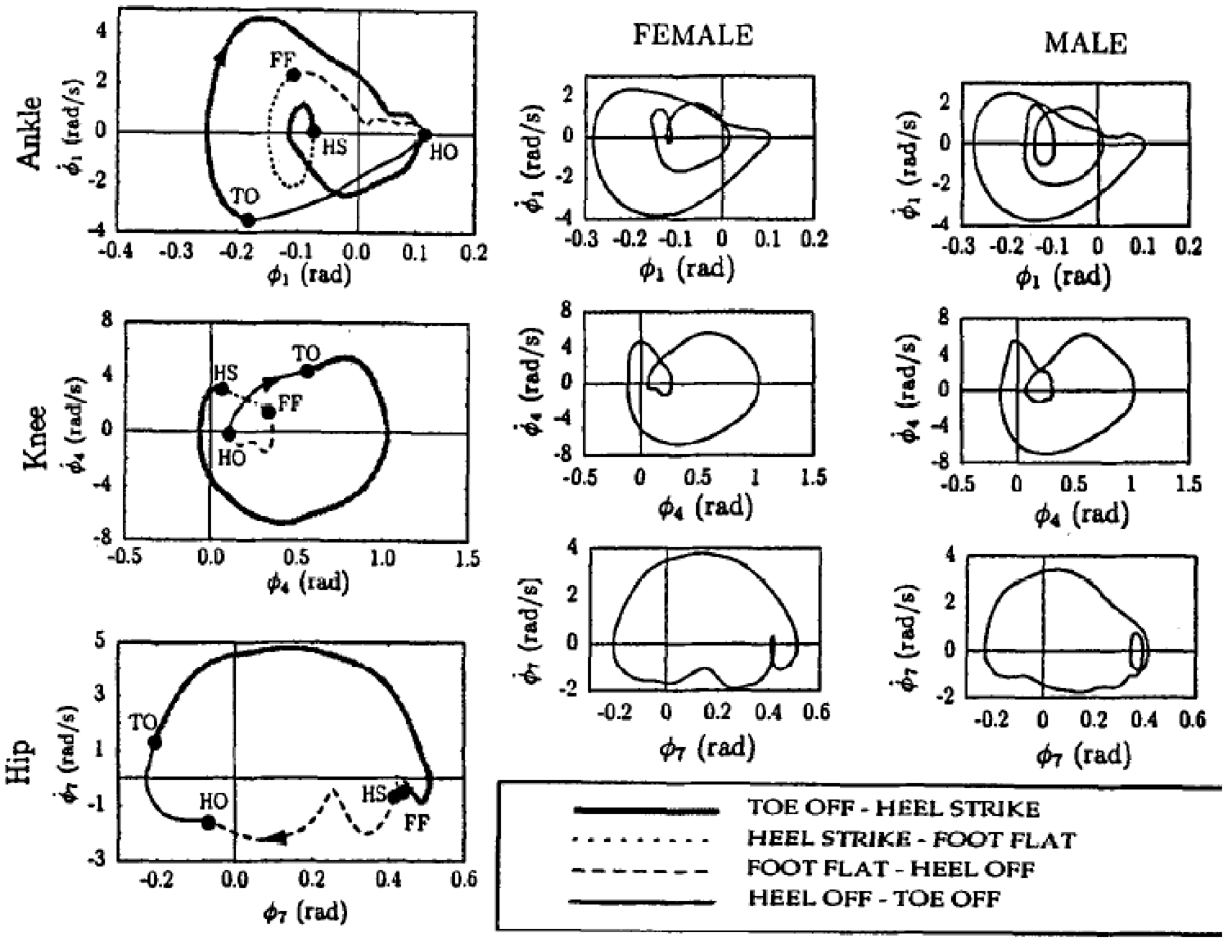

Fig. 3. (a) The detailed phase portraits of a typical female subject (the left column). (b) Phase portraits of healthy female subjects in sagittal plane (the middle column). (c) Phase portraits of healthy male subjects in sagittal plane (the right column). Phase plane portraits combine position and velocity data on a single plot. Steady state joint, velocities can be correlated directly with positions by eliminating the time variable.

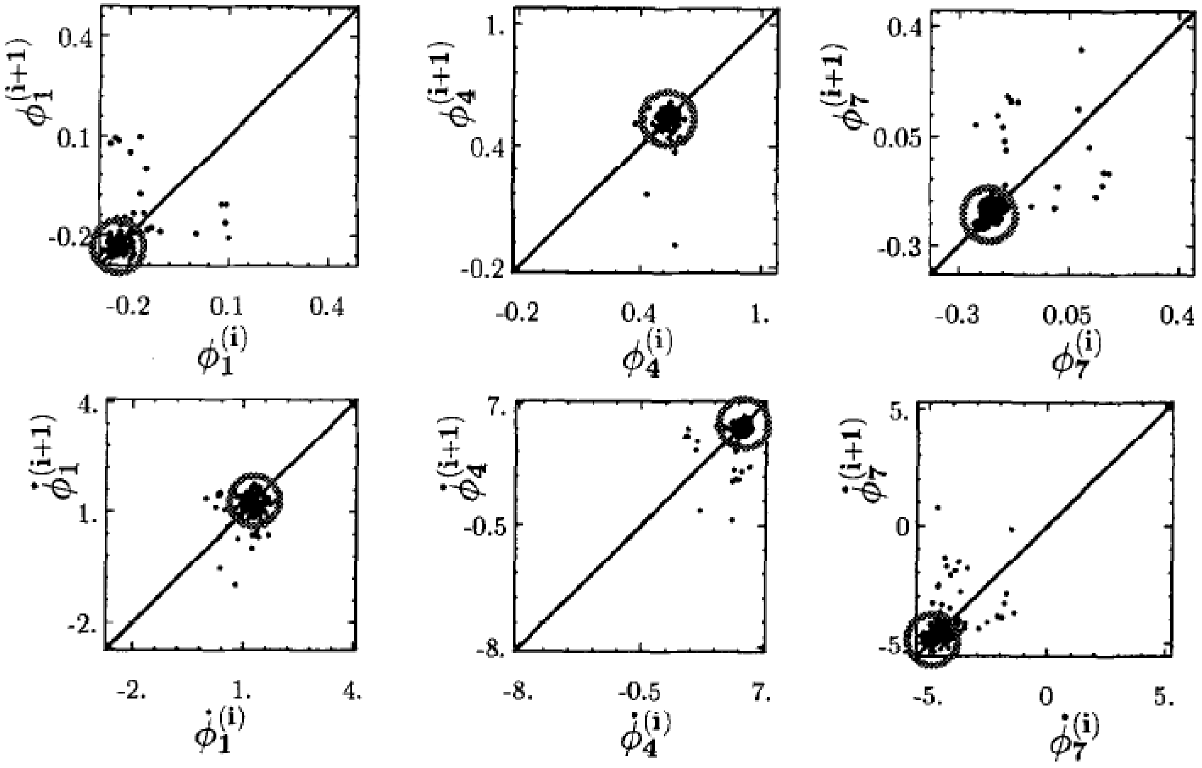

Fig. 4. Sagittal maps of a normal male subject. First return maps are graphical tools that facilitate in distinguishing between transient and steady state locomotion. Steady state locomotion can be observed from clustering of points inside the shown circles.

Hurmuzlu, Y., C. Basdogan, and J.J. Carollo, *Presenting joint kinematics of human locomotion using phase plane portraits and Poincare maps.* J Biomech, 1994. **27**(12): p. 1495-9.

Gait Cycle Analysis

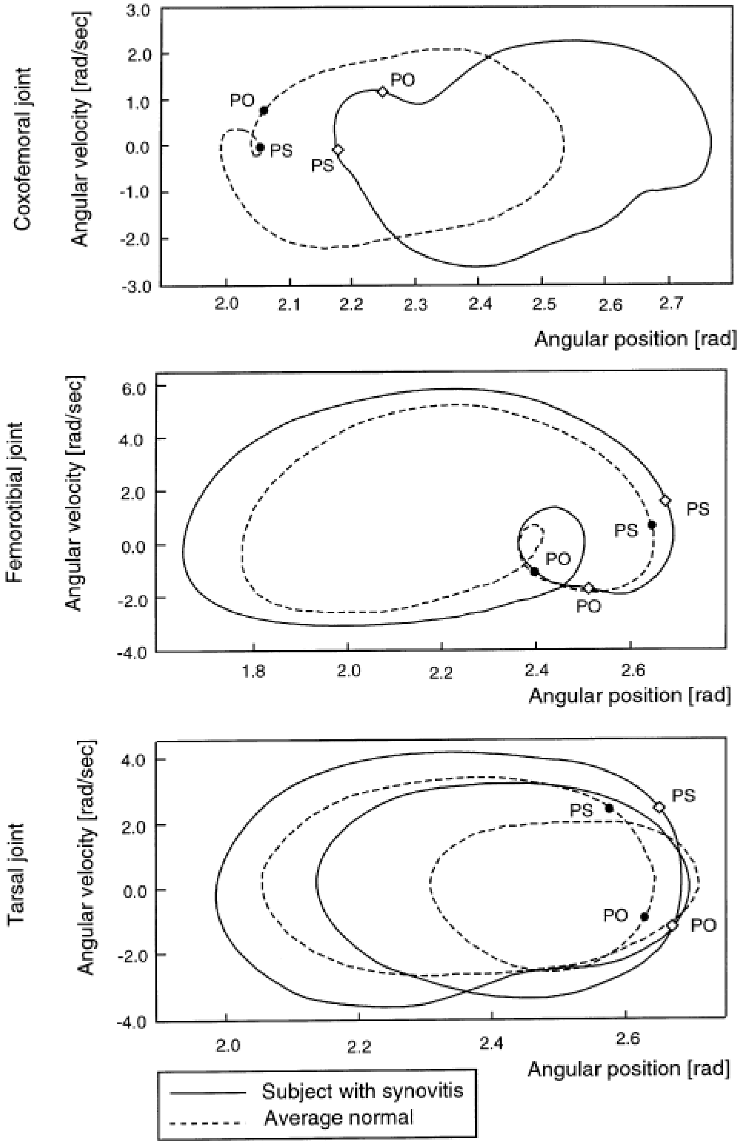

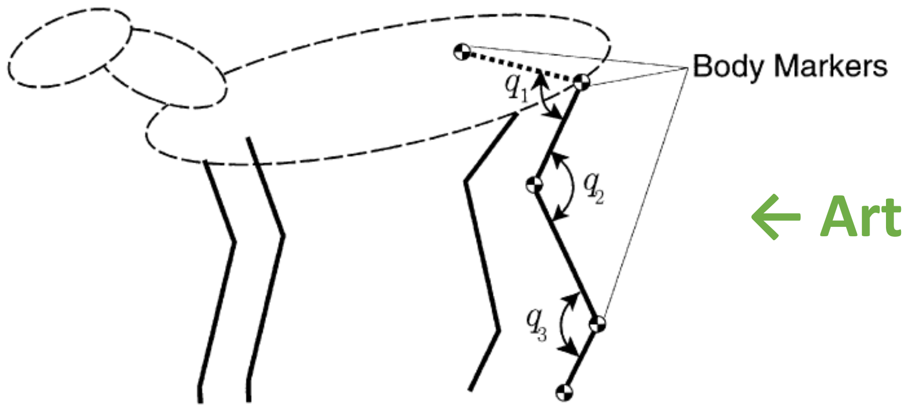

← Arthritic Greyhound

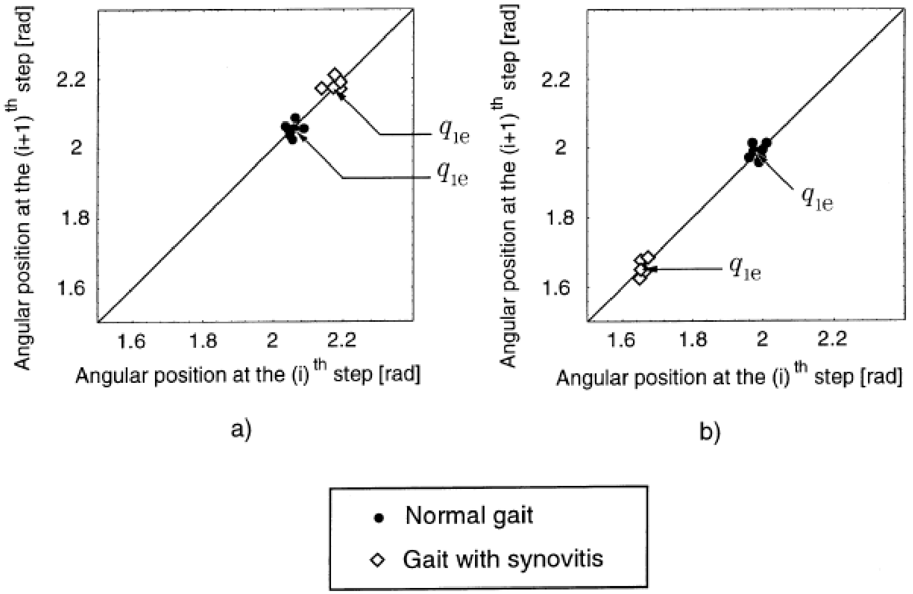

Figure 6. First return maps of coxofemoral joint rotations, (a) for subject 1, and (b) for subject 2, under conditions of normal gait and gait during acute synovitis. The angular position of the coxofemoral joint at equilibrium is denoted by q_{1e}.

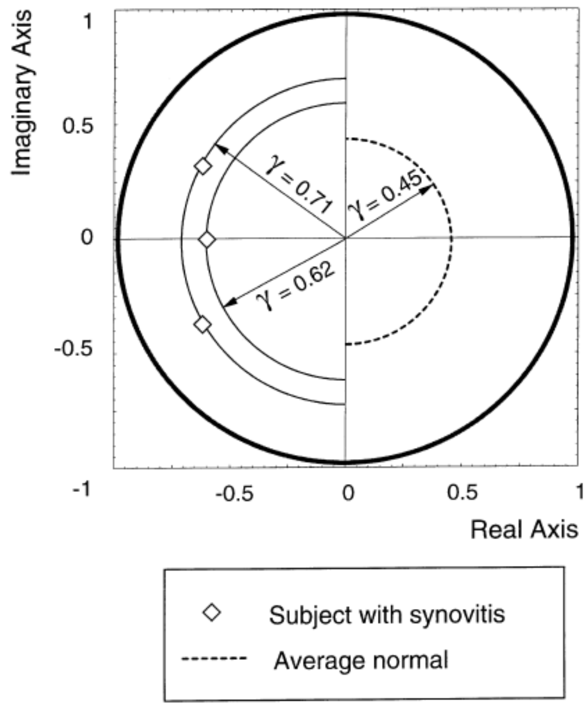

Figure 7. The stability index for greyhound locomotion.

Marghitu, D.B. and P. Nalluri, *Nonlinear dynamic stability of normal and arthritic greyhounds.* Nonlinear Dynamics, 1997. **12**(3): p. 237-250.

Circadian Rhythms

Limit Cycles

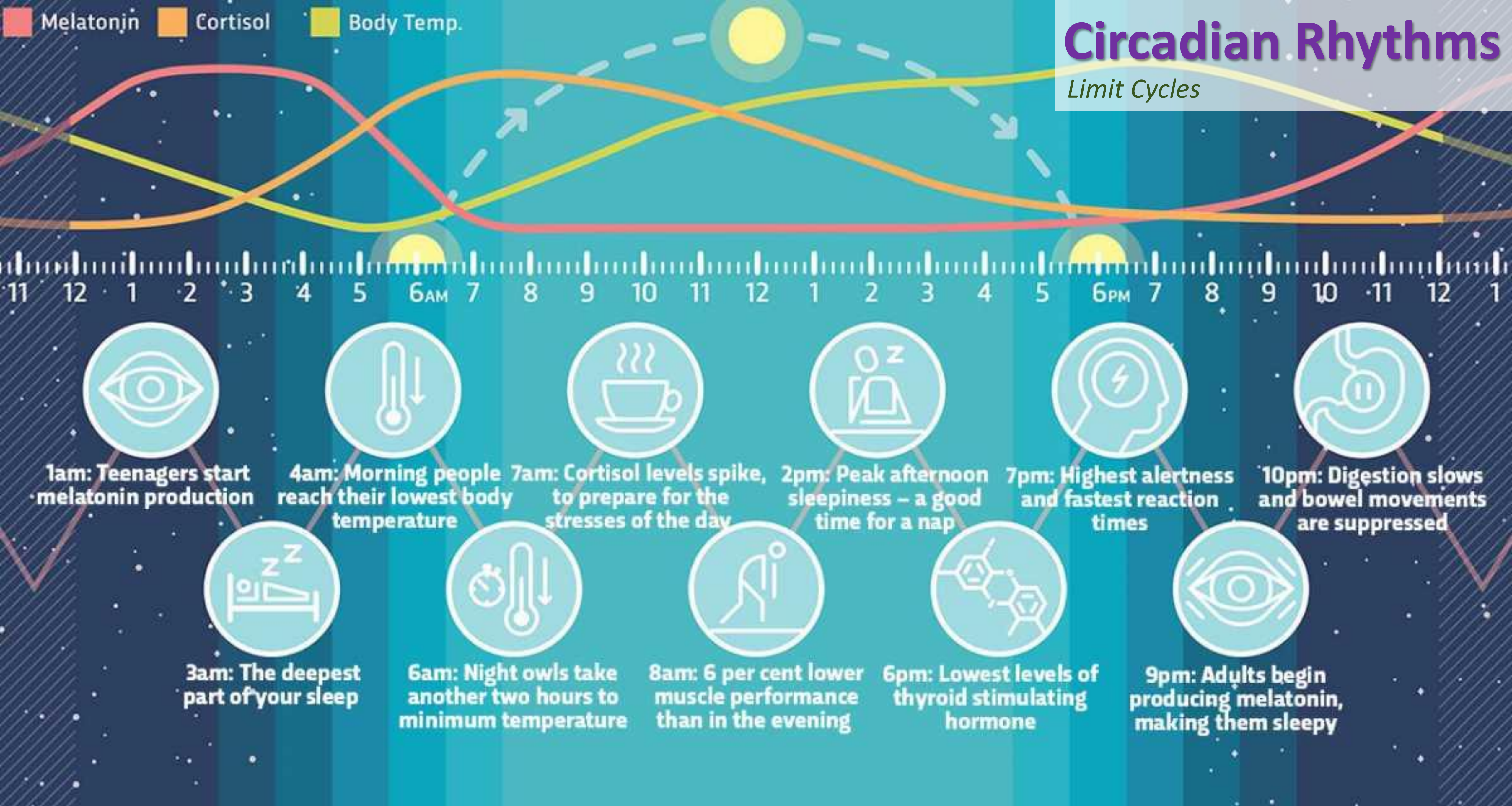

http://www.sciencefocus.com/article/human-body/how-do-circadian-rhythms-work

Circadian Rhythms

Kronauer 1990

$$\left(\frac{12}{\pi}\right)^2 \ddot{x} + \mu\left(4x^2 - 1\right)\left(\frac{12}{\pi}\right)\dot{x} + \left(\frac{24}{\tau_x}\right)^2 x = 0$$

$$\mu = 0.13 \quad \text{and} \quad \tau_x = 24.2$$

↓

$$\dot{x} = \left(\frac{\pi}{12}\right)\left[x_c + \mu\left(x - \frac{4}{3}x^3\right)\right]$$ Core Body Temp.

$$\dot{x}_c = -\left(\frac{\pi}{12}\right)\left(\frac{24}{\tau_x}\right)^2 x$$

Jewett 1999

$$\dot{x} = \left(\frac{\pi}{12}\right)\left[x_c + \mu\left(\frac{1}{3}x + \frac{4}{3}x^3 - \frac{256}{105}x^7\right) + B\right]$$

$$\dot{x}_c = \left(\frac{\pi}{12}\right)\left(qBx_c - \left[\left(\frac{24}{0.99729\tau_x}\right)^2 + kB\right]x\right)$$

Jewett, M.E., D.B. Forger, and R.E. Kronauer, *Revised limit cycle oscillator model of human circadian pacemaker.* J Biol Rhythms, 1999. **14**(6): p. 493-9.

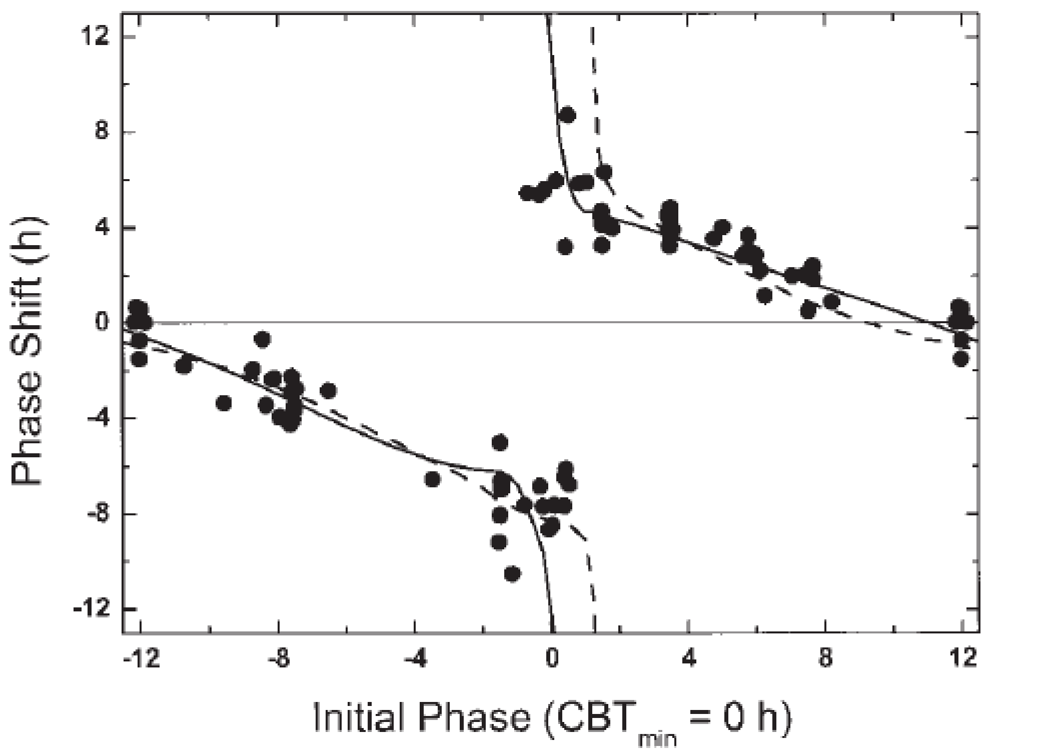

Figure 1. Phase response curves (PRC) to a three-cycle (5 h per cycle) bright light (~10,000 lux) stimulus. Initial phase is defined as the center of the light stimulus relative to the fitted minimum of the core body temperature measured during constant routine conditions (CBT$_{min}$), which is defined as 0 h. Simulations from Kronauer's (1990) model (dashed line) and our current model (solid line) are compared with experimental data (filled circles) from Khalsa et al. (1997). Note that one data point from that PRC was omitted because the subject (#1579) had undergone eye surgery prior to his experimental trial (Khalsa, personal communication, 1998).

Circadian Rhythms

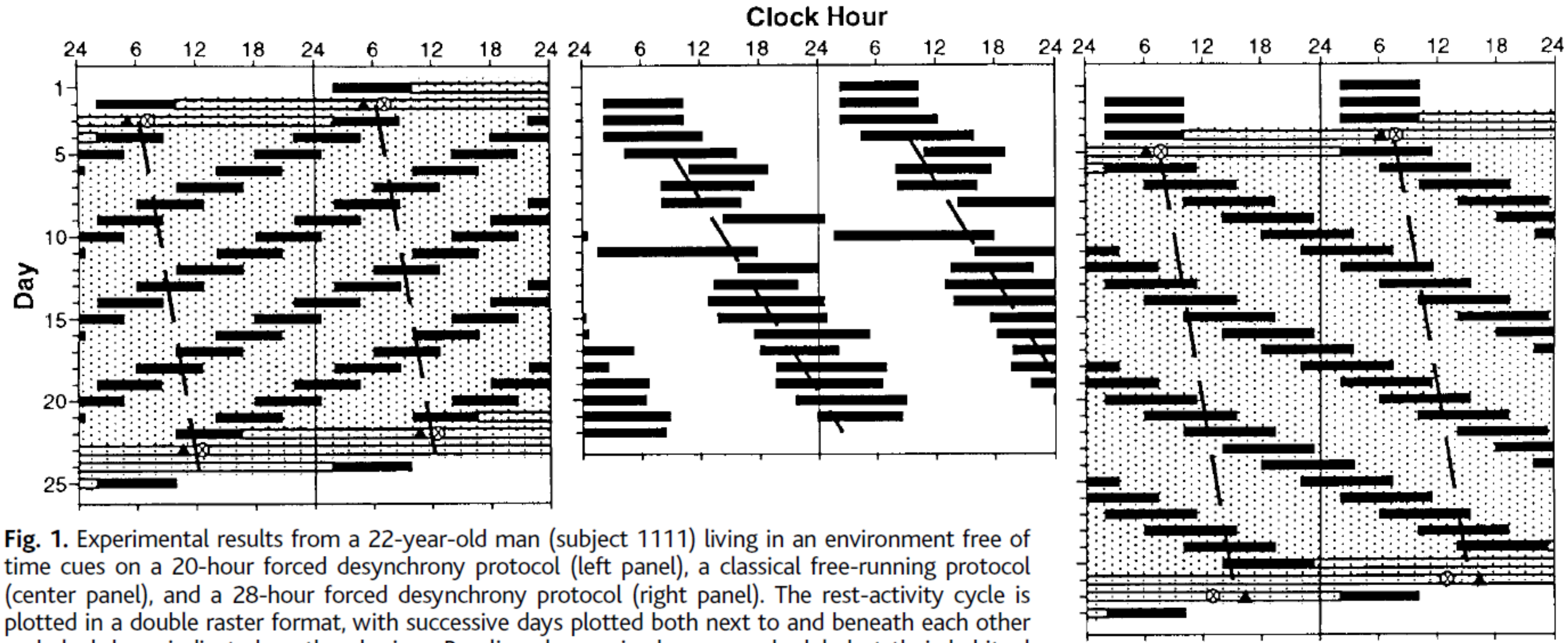

Fig. 1. Experimental results from a 22-year-old man (subject 1111) living in an environment free of time cues on a 20-hour forced desynchrony protocol (left panel), a classical free-running protocol (center panel), and a 28-hour forced desynchrony protocol (right panel). The rest-activity cycle is plotted in a double raster format, with successive days plotted both next to and beneath each other and clock hour indicated on the abscissa. Baseline sleep episodes were scheduled at their habitual times (based on an average of their schedule during the week before laboratory admission). Thereafter, sleep/dark episodes (solid bars, light intensity <0.03 lux) were scheduled for 6.67 hours (33% of imposed day) in the 20-hour protocol, self-selected by subject (averaging 28% of cycle) in the free-running protocol, and scheduled for 9.33 hours (33% of imposed day) in the 28-hour protocol. During wake episodes, the light intensity was ~15 lux (20- and 28-hour protocols) or ~150 lux (free-running protocol). Constant routines (open bars) for phase assessments of the endogenous circadian temperature nadir (⊗) and the fitted melatonin maximum (▲) were conducted before and after forced desynchrony in all subjects except 1209, who began forced desynchrony immediately after the three baseline days. Period estimations were performed with the use of temperature data (continuously collected via rectal thermistor throughout all studies) and plasma melatonin and cortisol data (assayed from samples collected every 20 to 60 min during segments of the study in the 20- and 28-hour protocols). The estimated phase of the circadian temperature rhythm (dashed line) was determined by nonorthogonal spectral analysis (*31*, *32*). The temperature period estimates are nearly equivalent under both forced desynchrony protocols (20-hour protocol, 24.29 hours; 28-hour protocol, 24.28 hours), independent of the imposed rest-activity cycle. However, the estimated temperature period (25.07 hours) observed during free-running conditions (with self-selected rest-activity cycle averaging 27.07 hours) was much longer.

Czeisler, C.A., et al., *Stability, precision, and near-24-hour period of the human circadian pacemaker*. Science, 1999. **284**(5423): p. 2177-81.

Neural Pattern Generators

Limit Cycles, Phase Plane Analysis

https://www.citarella.com/media/catalog/product/cache/1/image/97a78116f02a369697db694bbb2dfa59/0/2/024011800000_02.jpg

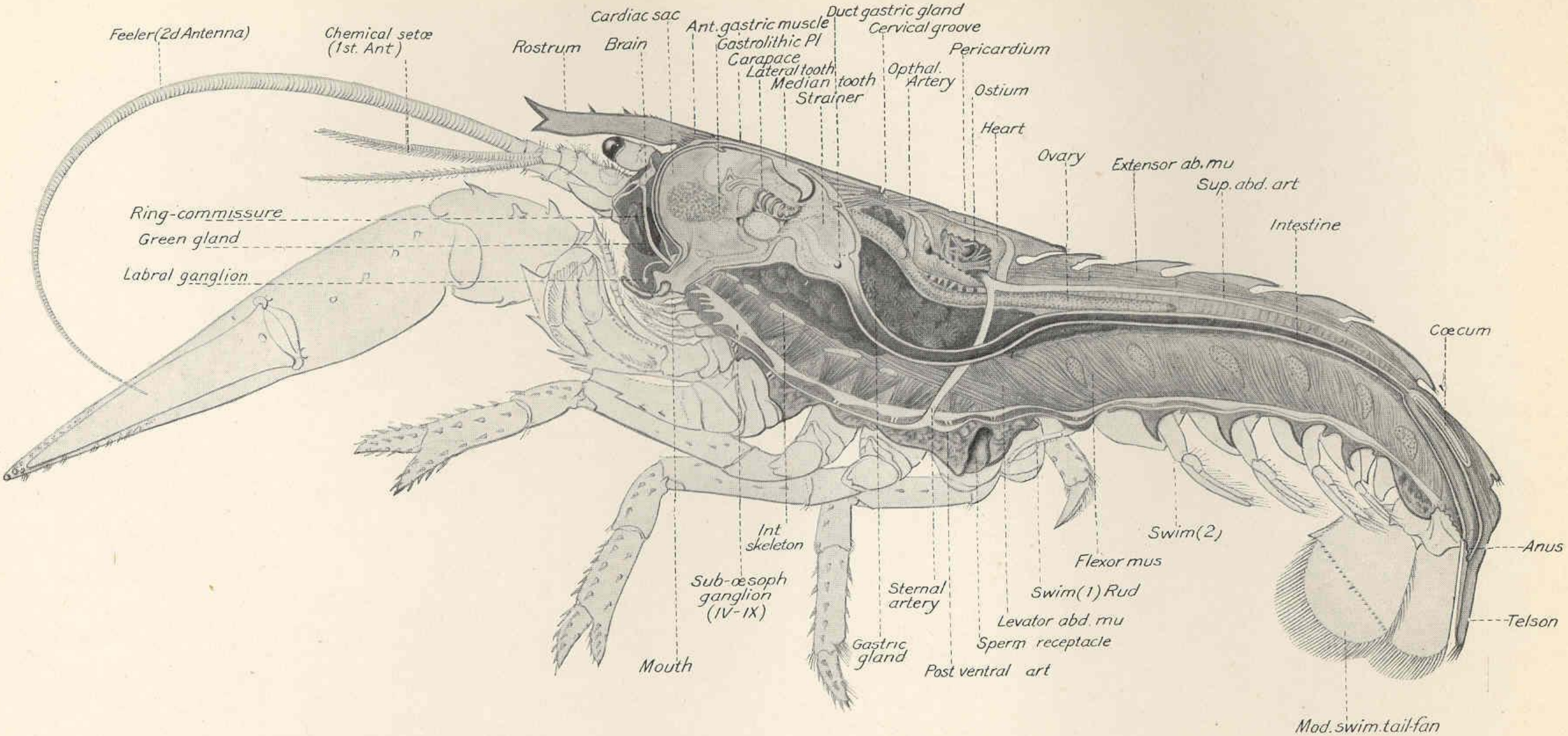

Half section of lobster cut in median plane to illustrate general anatomy. From soft shell female, 6½ inches long, slightly favored in head to show nervous system. Esophageal and gastric ganglion (the latter below reference line to anterior gastric muscle) and anterior visceral and median nerves are shown. Muscle marked levator abdominis (thoracico-abdominis) originates far forward in the thorax and joins enveloping muscles of the flexor system of abdomen. Note that abdominal sternal spines are much longer than in sexually mature animals.

Herrick, Francis Hobart (1911) *Natural History of the American Lobster*, Bulletin of the Bureau of Fisheries, vol.29, 1909, Washington, DC: Government Printing Office. Wikimedia Commons.


http://www.bio.brandeis.edu/marderlab/figures/gastricMill_col.jpg

Neural Pattern Generators

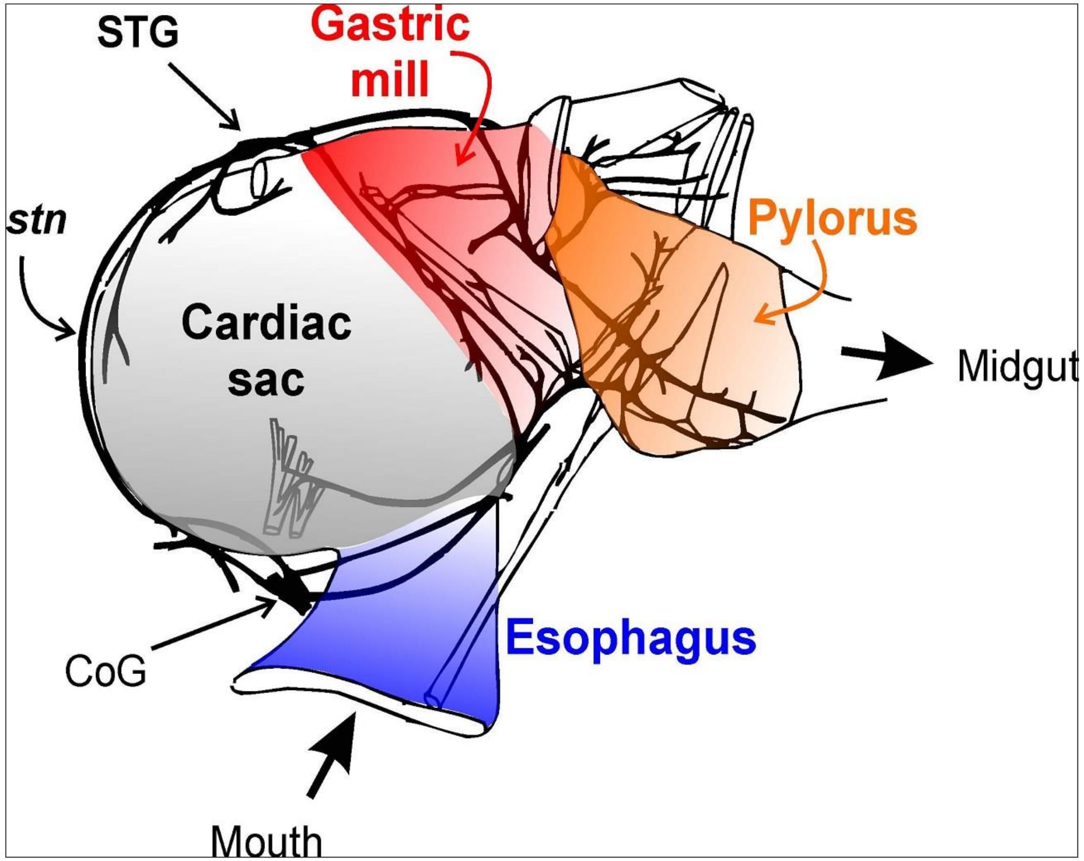

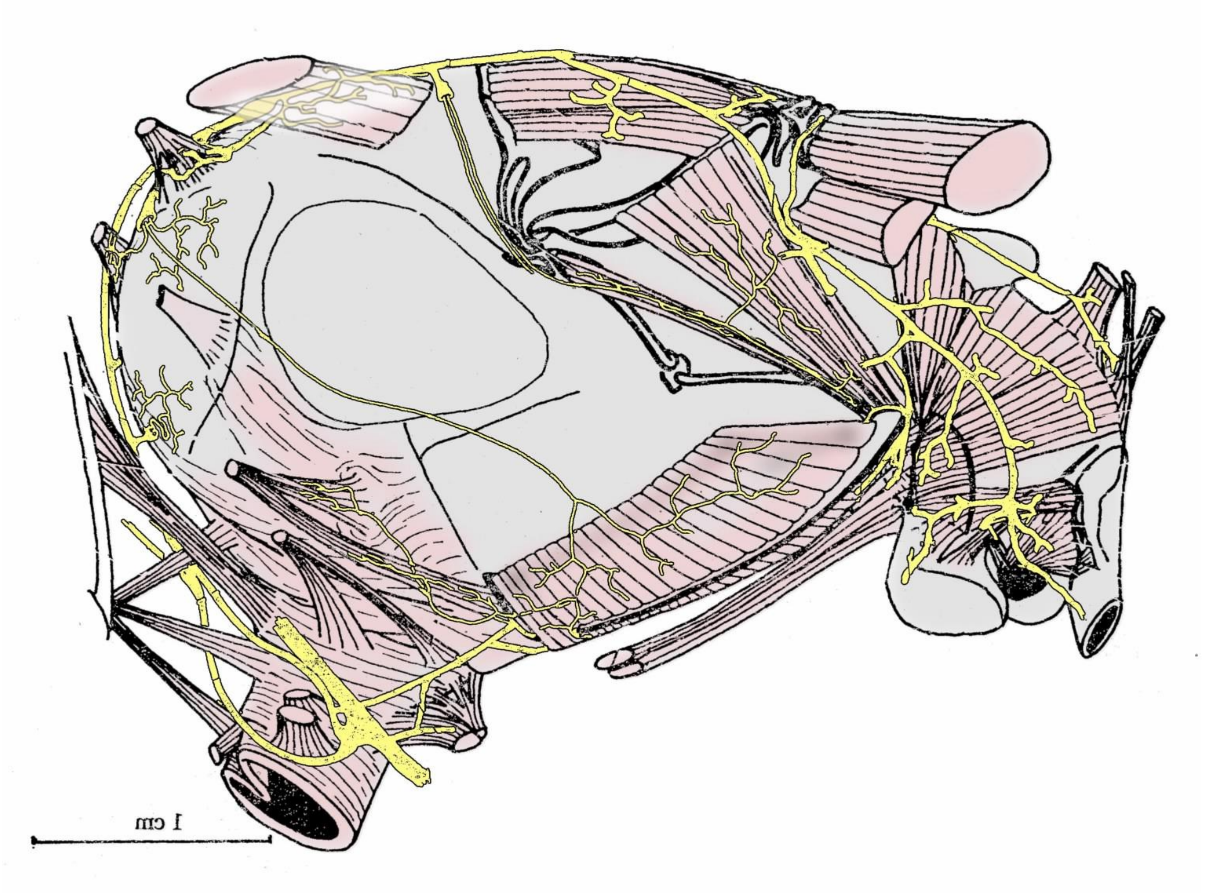

http://www.bio.brandeis.edu/marderlab/figures/gastricMill_col.jpg
http://www.bio.brandeis.edu/marderlab/figures/HomarusStomach.jpg

Neural Pattern Generators

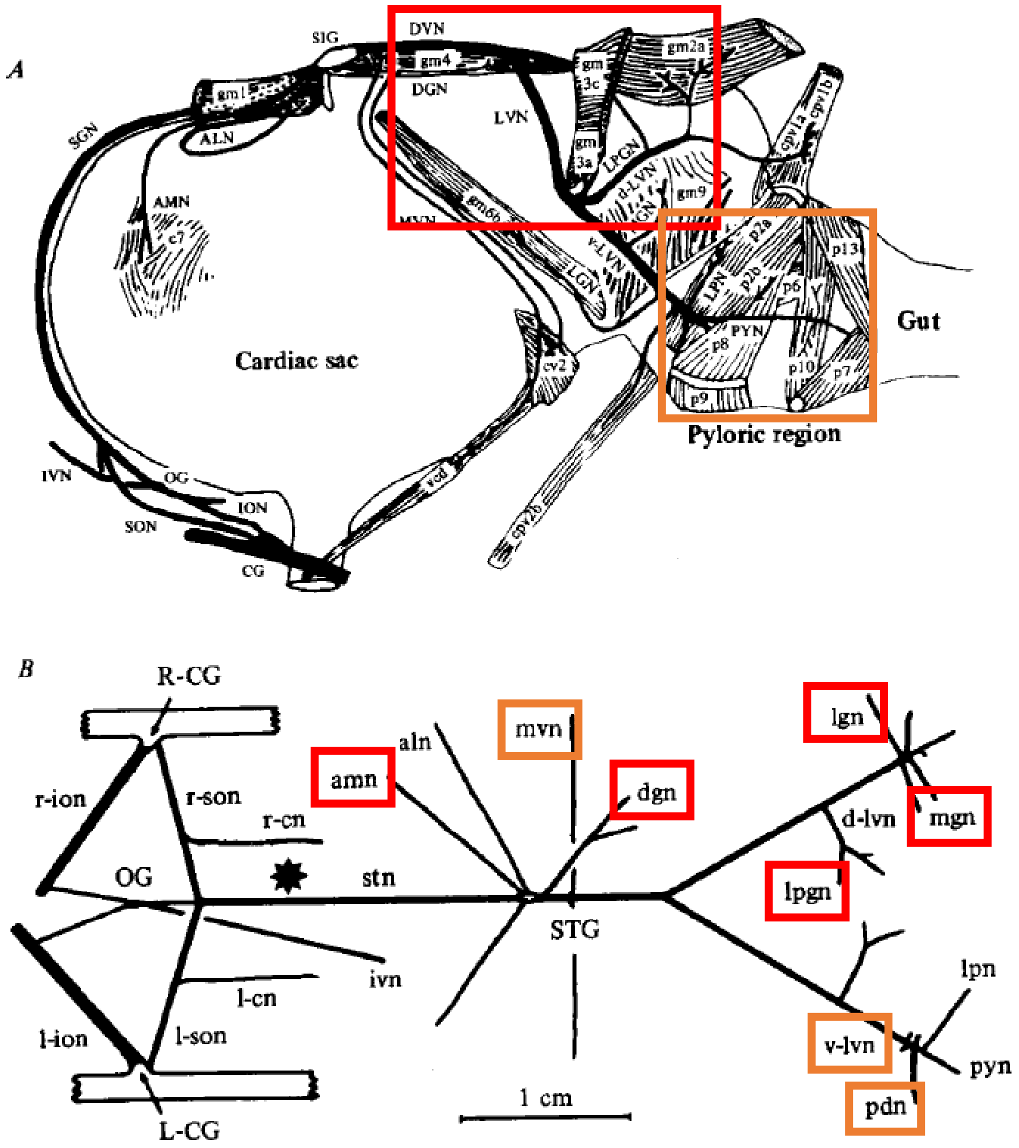

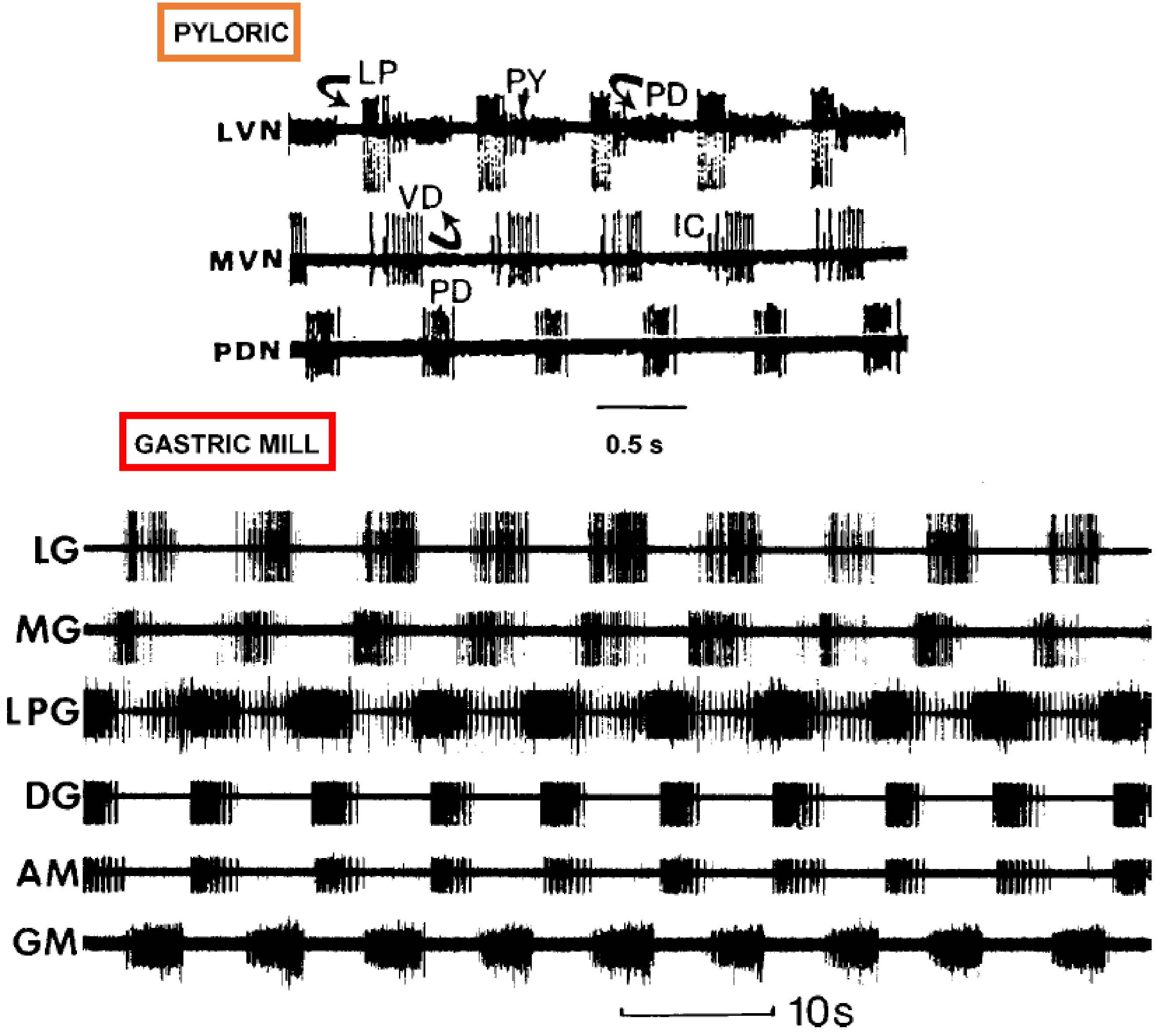

Selverston, A.I., *A neural infrastructure for rhythmic motor patterns.* Cell Mol Neurobiol, 2005. **25**(2): p. 223-44.

Neural Pattern Generators

- Studying the role of I_h in regulating pyloric and gastric mill cycles
- Phase portrait reveals rhythmic similarities in the absence of I_h
- Spontaneous recovery when blocking relaxed -> limit cycle

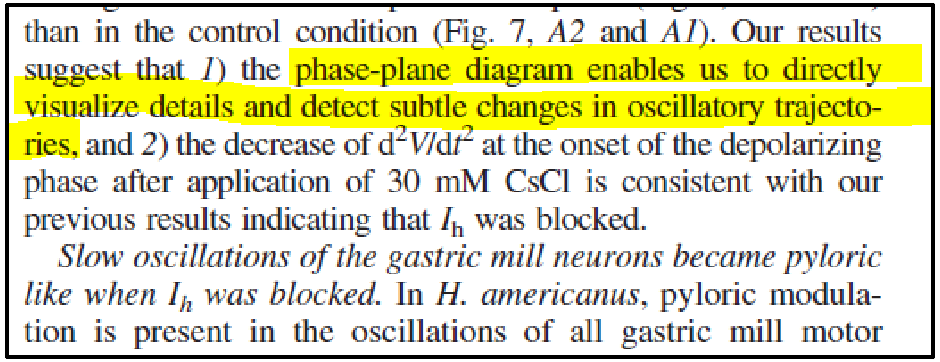
than in the control condition (Fig. 7, *A2* and *A1*). Our results suggest that *1*) the phase-plane diagram enables us to directly visualize details and detect subtle changes in oscillatory trajectories, and 2) the decrease of d^2V/dt^2 at the onset of the depolarizing phase after application of 30 mM CsCl is consistent with our previous results indicating that I_h was blocked.

Slow oscillations of the gastric mill neurons became pyloric like when I_h was blocked. In *H. americanus*, pyloric modulation is present in the oscillations of all gastric mill motor

Pyloric Neurons

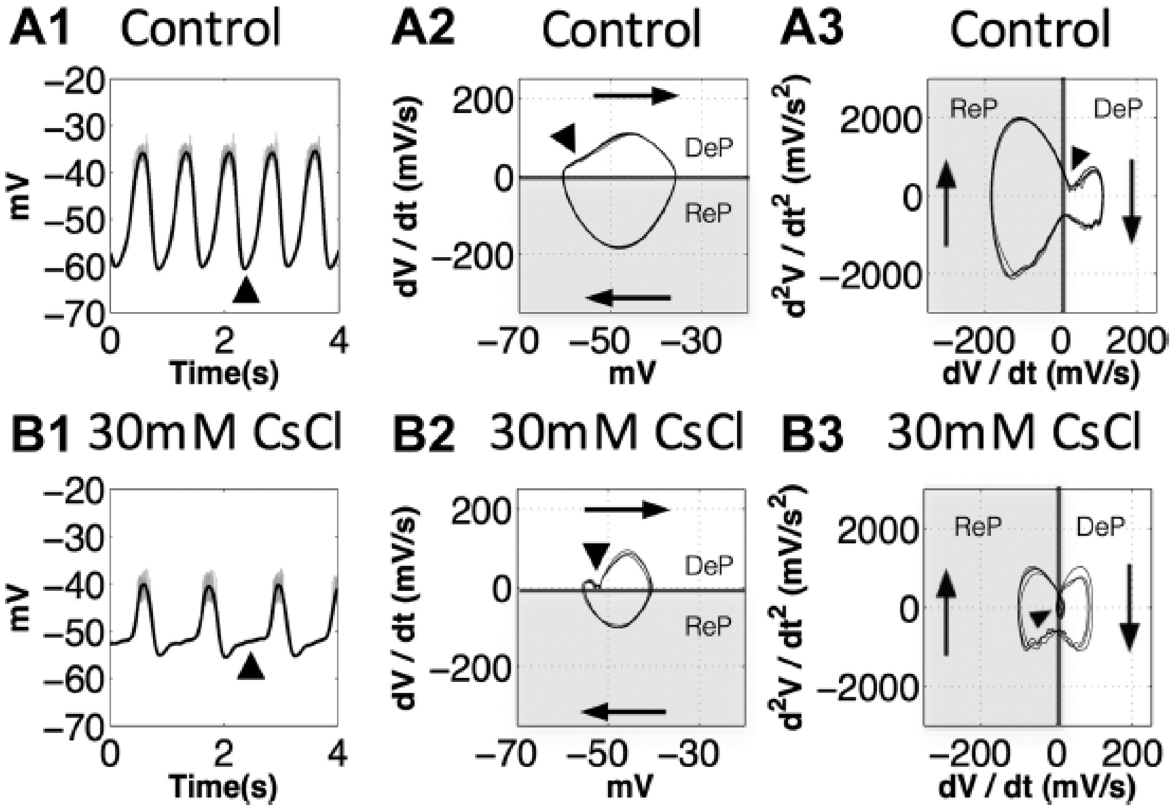

Gastric Mill Neurons

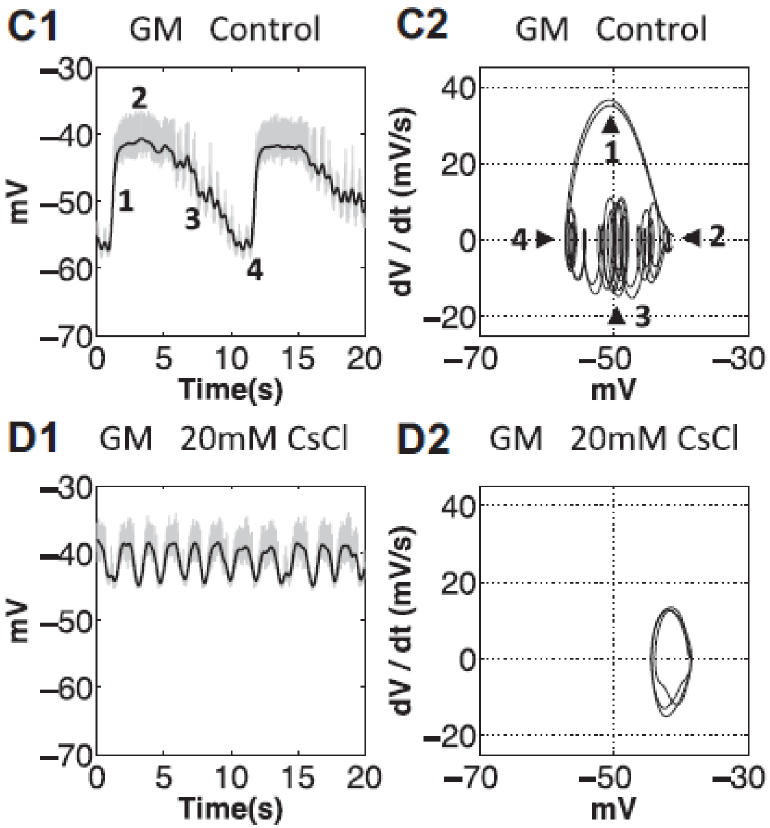

Zhu, L., A.I. Selverston, and J. Ayers, *Role of Ih in differentiating the dynamics of the gastric and pyloric neurons in the stomatogastric ganglion of the lobster, Homarus americanus.* J Neurophysiol, 2016. **115**(5): p. 2434-45.

Cardiac Pacing

Limit Cycles, Poincaré Maps

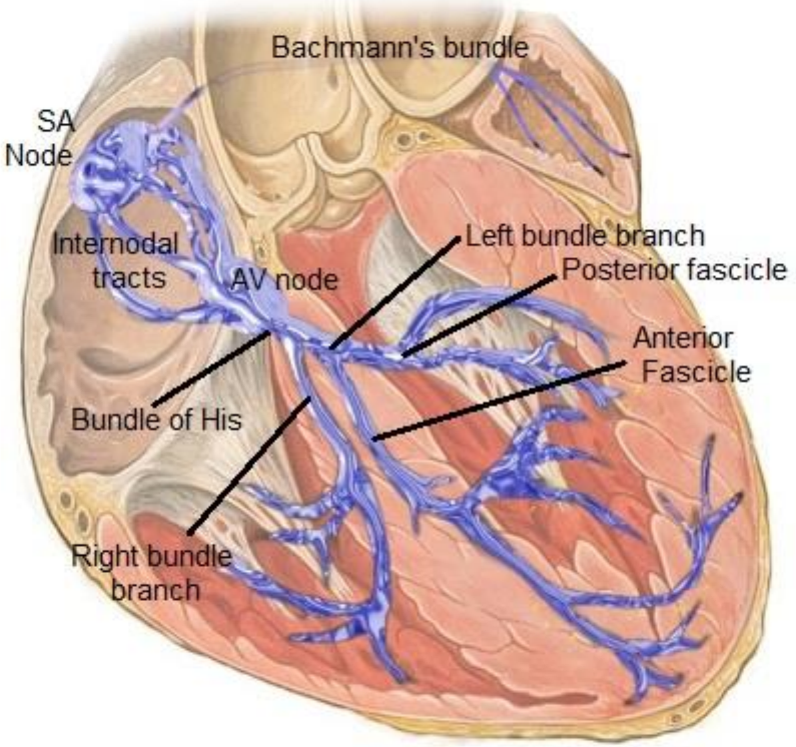

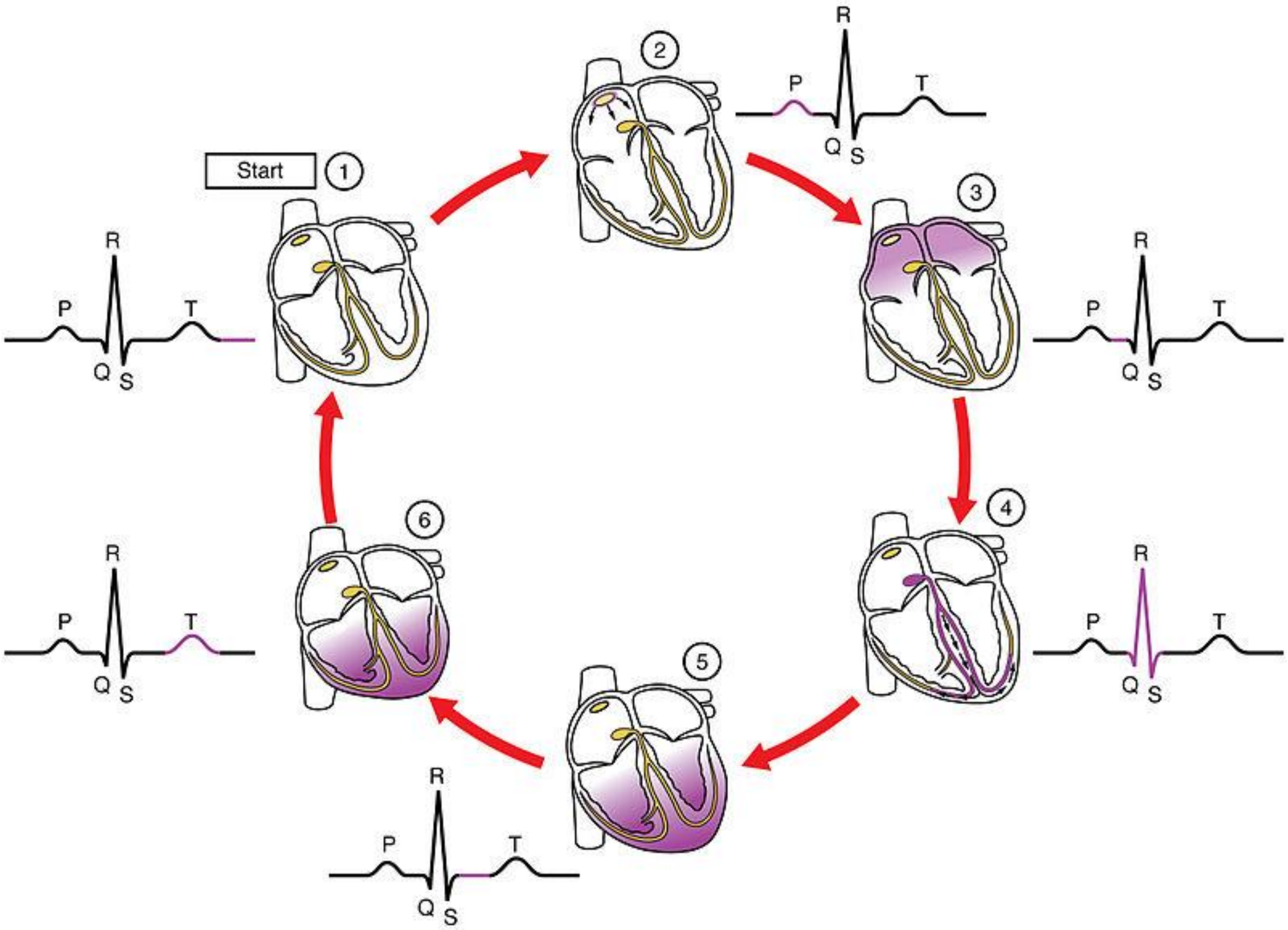

https://commons.wikimedia.org/wiki/File:Cardiac_conduction_system.jpg
https://commons.wikimedia.org/wiki/File:2023_ECG_Tracing_with_Heart_ContractionN.jpg

Cardiac Pacing

1 Period

2 Periods

4 Periods

Aperiodic (Chaotic)

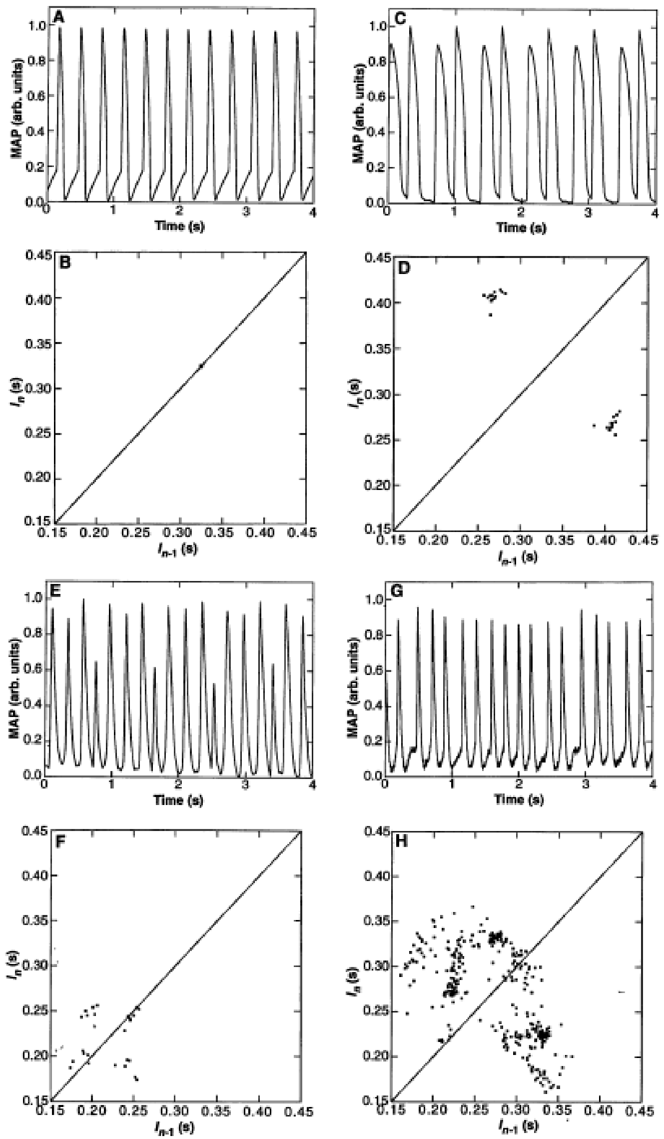

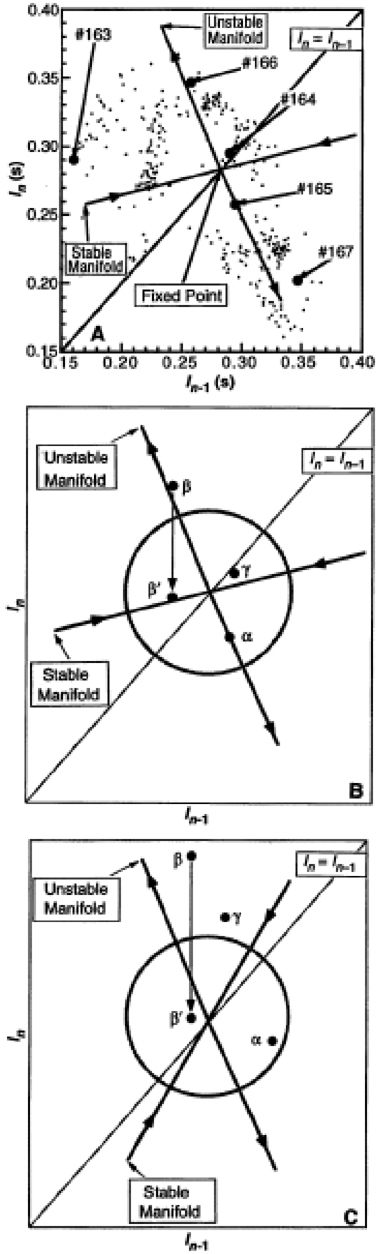

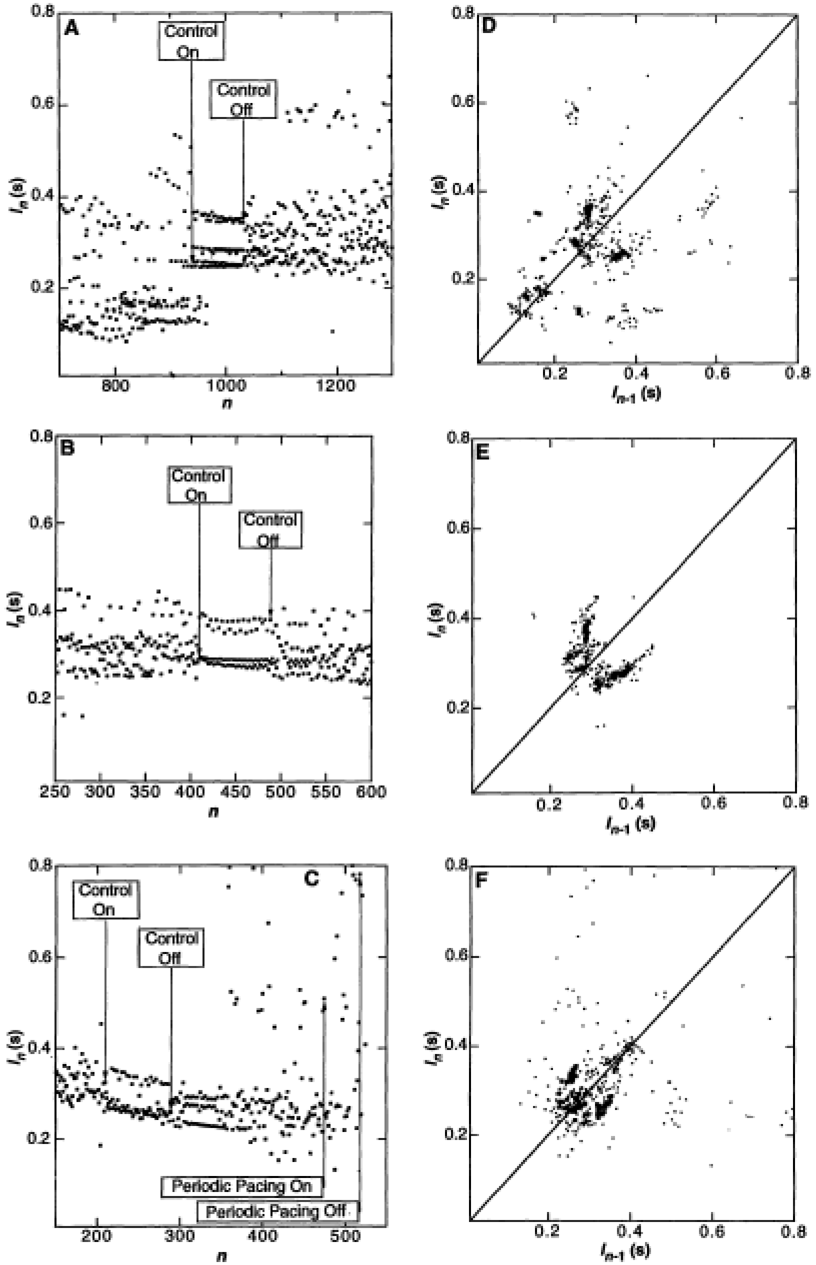

Garfinkel, A., et al., *Controlling cardiac chaos.* Science, 1992. **257**(5074): p. 1230-5.
Crutchfield, J.P., et al., *Chaos.* Scientific American, 1986. **255**(6): p. 46-&.

Pushing the Limit (Cycle)

- Graphical methods can provide insight into the structure of nonlinear dynamical systems, even when differential equations cannot be solved analytically
- Limit cycles possible in nonlinear systems
- Periodic (and aperiodic) oscillations in biological systems can be analyzed - and sometimes controlled - using nonlinear techniques

Dartmouth Biomedical Engineering Center

PI: Dr. Douglas Van Citters

Rebecca Butler
Ryan Chapman
Dr. John Collier
Barb Currier
John Currier
Audrey Martin
Dr. Michael Mayor, MD
Fioleda Prifti

Next up: Chaos in the OR?